Chapter 7

Parameterization-Averaged Subgrid-Scale Fluxes

The grid-volume averaging of the conservation relations as described in Chapters 4 and 6 results in averaged subgrid-scale correlation terms [e.g., $\rho_0 \overline{u_j'' u_i''}$ from Eq. (4-21)] and averaged source–sink terms [e.g., $\overline{S}_\theta$ from Eq. (4-24)]. In the following three chapters, the representation in mesoscale models of three types of physical processes are introduced. This specification of subgrid-scale and source–sink processes using experimental data and simplified fundamental concepts is called *parameterization*. Usually the parameterizations are not defined in terms of basic conservation principles. A parameterization does not necessarily have to actually simulate the physical processes that it is representing to be a realistic representation of these terms.

Indeed, if the quantitative accuracy of a parameterization is not sacrificed, then it is desirable to make the parameterization as computationally simple as possible. The three processes to be parameterized are

- averaged subgrid-scale fluxes [i.e., $\rho_0 \overline{u_j'' u_i''}$, $\rho_0 \overline{u_j'' \theta}$, etc., in Eqs. (4-21) and (4-24)–(4-26)]
- averaged radiation flux divergence [i.e., part of $\overline{S}_\theta$ in Eq. (4-24)]
- averaged effects of the change of phase of water, including precipitation [i.e., $\overline{S}_{q_n}$ in Eq. (4-25), part of $\overline{S}_\theta$ in Eq. (4-24)].

The averaged effects of change of phase, precipitation, and/or change into other chemical species of atmospheric gases and aerosols other than water [i.e., S_{χ_m} in Eq. (4-26)] is not covered in this text. The reader is referred to Seinfeld (1975) and Seinfeld and Pandis (1997) for reports on the status of parameterizing these complex effects.

This chapter describes the parameterization of the averaged vertical subgrid fluxes. As discussed in Section 10.5 in Chapter 10, horizontal subgrid-scale fluxes are used only for computational reasons, since little is known of

horizontal subgrid-scale mixing on the mesoscale (or in other models whenever $\Delta x; \Delta y \gg \Delta z$), although work for ocean mixing, such as that of Young *et al.* (1982), offers an avenue for future research. As discussed in Chapter 4, the magnitude of the subgrid-scale variables and fluxes often can be the same or even larger than the resolvable dependent variables. A wind gust of 5 m s^{-1} (representing u''), for example, is not uncommon with an average wind speed of 5 m s^{-1} (representing $\bar{u}$). Figure 7-1 schematically illustrates a subgrid-scale correlation between vertical velocity and potential temperature. In this example, assumed to be close to flat ground so the grid-volume–averaged vertical velocity is approximately 0 (i.e., $\bar{w} \simeq 0$), the ground surface is assumed to be warmer than the air above, so that an upward perturbation vertical velocity tends to transport warm air upward, whereas descending motion tends to advect cooler air downward.[1] Averaging over the grid interval in this example yields an upward flux of heat ($\overline{w''\theta''} > 0$ with a magnitude of 6.9 cm K s^{-1}). Thus, despite the insignificant vertical flux of heat associated with the resolvable dependent variables (i.e., $\bar{w}\bar{\theta} \simeq 0$, since $\bar{w} \simeq 0$), a substantial transport of heat will occur because of the positive correlation between the subgrid-scale vertical velocity and potential temperature perturbation.

In developing subgrid-scale averaged quantities, however, one must recognize that the preferred representation is an ensemble average over the grid volume, rather than simply the grid-volume average as defined by Eq. (4-6). The ensemble average represents the most likely value of the subgrid-scale quantity, whereas the grid-volume average represents just one realization. Unless the subgrid-scale quantity is completely deterministic (i.e., without a statistical component), the two averages will not in general be the same. Thus in the parameterizations discussed in this chapter, it is assumed that they are the most

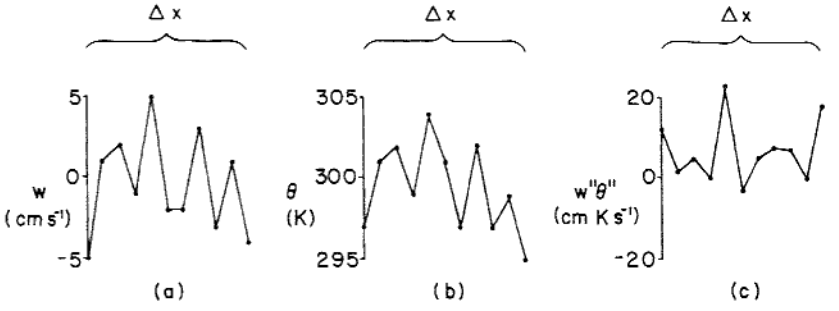

Fig. 7-1. Schematic illustration of subgrid-scale values of vertical velocity, w, potential temperature, θ, and the subgrid-scale correlation, $w''\theta''$. In this example, the grid-averaged value of vertical motion is required to be approximately 0 (i.e., $\bar{w} \simeq 0$), and $\bar{\theta} = 299.5$ K is used. Both grid value averages are assumed to be constant over Δx. The grid-averaged subgrid-scale correlation $\overline{w''\theta''}$ is equal to 6.9 cm K s^{-1}.

likely (i.e., ensemble) estimates. Wyngaard (1982, 1983) and Cotton and Anthes (1989) discuss ensemble averaging in more depth. Defining a parameterization in terms of a realization from a probability distribution is an area meriting future research. Preliminary work in this area has been completed, as reported in Garratt and Pielke (1989), Garratt *et al.* (1990), and Avissar (1991, 1992).

7.1 Basic Terms

To develop parameterization for these subgrid-scale correlations, it is necessary to introduce several basic definitions. To simplify the interpretation, a Cartesian coordinate framework is applied in this analysis. Modifications for when a generalized vertical coordinate system is used were discussed in Chapter 6.

Neglecting the Coriolis effect, Eq. (4-4) can be rewritten as

$$\frac{\partial}{\partial t}(\bar{u}_i + u_i'') = -(\bar{u}_j + u_j'')\frac{\partial}{\partial x_j}(\bar{u}_i + u_i'') - (\theta_0 + \theta' + \theta'')\frac{\partial(\bar{\pi} + \pi'')}{\partial x_i} - g\delta_{i3}, \tag{7-1}$$

where Eq. (4-36) is used to represent the pressure gradient force, with θ and π decomposed using the definitions given by Eqs. (4-3) and (4-12). Assuming that the synoptic-scale variables are in hydrostatic equilibrium, and that fluctuations in potential temperature (i.e., θ' and θ'') are neglected relative to θ_0 except when multiplied by gravity,[2] Eq. (7-1) can be rewritten as

$$\frac{\partial}{\partial t}(\bar{u}_i + u_i'') = -(\bar{u}_j + u_j'')\frac{\partial}{\partial x_j}(\bar{u}_i + u_i'') - \theta_0\frac{\partial(\pi' + \pi'')}{\partial x_i} - \theta_0\left[\frac{\partial \pi_0}{\partial x}\delta_{i1} + \frac{\partial \pi_0}{\partial y}\delta_{i2}\right] + \frac{g\theta'}{\theta_0}\delta_{i3} + \frac{g\theta''}{\theta_0}\delta_{i3}. \tag{7-2}$$

Averaging this equation over a grid volume using Eq. (4-6) and applying the assumptions given by Eq. (4-8) yields

$$\frac{\partial \bar{u}_i}{\partial t} = -\bar{u}_j\frac{\partial}{\partial x_j}\bar{u}_i - \overline{u_j''\frac{\partial}{\partial x_j}u_i''} - \theta_0\frac{\partial \pi'}{\partial x_i} - \theta_0\left[\frac{\partial \pi_0}{\partial x}\delta_{i1} + \frac{\partial \pi_0}{\partial y}\delta_{i2}\right] + g\frac{\theta'}{\theta_0}\delta_{i3}. \tag{7-3}$$

Subtracting Eq. (7-3) from (7-2) gives

$$\frac{\partial u_i''}{\partial t} = -\bar{u}_j \frac{\partial}{\partial x_j} u_i'' - u_j'' \frac{\partial u_i''}{\partial x_j} - u_j'' \frac{\partial \bar{u}_i}{\partial x_j} + \overline{u_j'' \frac{\partial u_i''}{\partial x_j}} - \theta_0 \frac{\partial \pi''}{\partial x_i} + g \frac{\theta''}{\theta_0} \delta_{i3}, \qquad (7\text{-}4)$$

which is a prognostic equation for the subgrid-scale velocity perturbation.

Multiplying Eq. (7-4) by u_i'', averaging using Eq. (4-6), and applying the assumption[3] $\overline{u_i''} = 0$ results in

$$\frac{\partial \bar{e}}{\partial t} = -\bar{u}_j \frac{\partial \bar{e}}{\partial x_j} - \overline{u_j'' \frac{\partial e}{\partial x_j}} - \overline{u_j'' u_i''} \frac{\partial \bar{u}_i}{\partial x_j} - \theta_0 \overline{u_i'' \frac{\partial \pi''}{\partial x_i}} + g \frac{\overline{u_i'' \theta''}}{\theta_0} \delta_{i3}, \qquad (7\text{-}5)$$

where $\bar{e} = \frac{1}{2} \overline{u_i''^2}$ and $e = \frac{1}{2} u_i''^2$. In the context of a numerical model, Eq. (7-5) is the grid-volume–averaged, subgrid-scale perturbation kinetic energy equation. This equation is usually called the *turbulent kinetic energy equation*,[4] with $\bar{e}$ the average turbulent kinetic energy.[5] The individual terms in Eq. (7-5) have the interpretation given in Table 7-1.

TABLE 7-1.

An Interpretation of the Individual Terms in Eq. (7-5)[a]

Term	Interpretation
$\frac{\partial \bar{e}}{\partial t}$	Local grid-volume change of averaged subgrid-scale perturbation kinetic energy $\bar{e}$
$\bar{u}_j \frac{\partial \bar{e}}{\partial x_j}$	Advection of $\bar{e}$ by the grid-volume–averaged velocity
$\overline{u_j'' \frac{\partial e}{\partial x_j}}$	Grid-volume–averaged advection of e by the subgrid-scale perturbation velocity
$\overline{u_j'' u_i''} \frac{\partial \bar{u}_i}{\partial x_j}$	Extraction from or input to $\bar{e}$ from the existence of both an average velocity shear and subgrid-scale velocity fluxes; also referred to as the *shear production* of turbulent kinetic energy
$\theta_0 \overline{u_i'' \frac{\partial \pi''}{\partial x_i}}$	Multiplying this term by ρ_0 and assuming that the anelastic conservation-of-mass equation is valid for the subgrid scale (i.e., $(\partial/\partial x_i)\rho_0 u_i'' = 0$) yields $\theta_0(\partial/\partial x_i)\,\rho_0 \overline{u_i'' \pi''}$. Therefore, when the anelastic assumption is valid, this term causes changes in $\bar{e}$ only by advection through the boundaries of the grid volume. As discussed by Lumley and Panofsky (1964), the influence of the correlation between the turbulent velocity and pressure variables is to transfer kinetic energy between the three velocity components.
$g \frac{\overline{u_i'' \theta''}}{\theta_0} \delta_{i3} = g \frac{\overline{w'' \theta''}}{\theta_0}$	Extraction or production of $\bar{e}$ by buoyancy; referred to as the *buoyant production* of turbulent kinetic energy

[a] Lumley and Panofsky (1964), from which the derivation of Eq. (7-5) was based, discuss the turbulent kinetic energy equation and its derivation in detail.

If Eq. (7-5) were used to simulate the details of turbulence in a model, then the molecular dissipation of average turbulent kinetic energy would be included to guarantee a sink for this energy. In a mesoscale model, however, as discussed in Section 10.6, computational devices such as horizontal filters are applied to prevent the artificial accumulation of kinetic energy at short wavelengths. Such mechanisms are necessitated by the inability to resolve both the mesoscale and the small spatial scales in which the molecular dissipation of kinetic energy becomes significant.[6]

To contrast the relative contribution of the two source–sink terms of $\bar{e}$ in Eq. (7-5), it is useful to define the ratio

$$R_f = \frac{g}{\theta_0} \overline{w''\theta''} \Big/ \left[\overline{w''u''} \frac{\partial \bar{u}}{\partial z} + \overline{w''v''} \frac{\partial \bar{v}}{\partial z} \right], \tag{7-6}$$

where R_f is called the *flux Richardson number*. In this expression, horizontal contributions to the shear production of $\bar{e}$ are neglected and $|\partial \bar{u}/\partial z| \simeq |\partial \bar{v}/\partial z| \gg |\partial \bar{w}/\partial z|$. The flux Richardson number is a measure of the relative contribution of the buoyant production or dissipation of averaged, subgrid-scale kinetic energy relative to its generation or extraction by the vertical shear of the averaged horizontal wind.

In analogy with the molecular fluxes of heat and momentum [e.g., Eq. (3-29)], the vertical subgrid-scale flux terms $\overline{w''\theta''}$, $\overline{w''u''}$, and $\overline{w''v''}$ are often represented by

$$\begin{aligned} &\overline{w''\theta''} = -K_\theta \frac{\partial \bar{\theta}}{\partial z}, \qquad \overline{w''q_k''} = -K_\theta \frac{\partial \bar{q}_k}{\partial z}, \qquad \overline{w''\chi_m''} - K_\theta \frac{\partial \overline{\chi}_m}{\partial z}, \\ &\overline{w''u''} = -K_m \frac{\partial \bar{u}}{\partial z}, \qquad \text{and} \qquad \overline{w''v''} = -K_m \frac{\partial \bar{v}}{\partial z}, \end{aligned} \tag{7-7}$$

as assumed, for example, by Eq. (5-3), where K_θ and K_m are referred to as *exchange coefficients*. This form of representing the grid-volume subgrid-scale fluxes is called *first-order closure*. As discussed later in this section, however, it is important to note that although molecular mixing is a function of the type of fluid involved, turbulent mixing, such as represented by Eq. (7-7), is a function of the flow. Therefore, the turbulent exchange coefficients K_θ and K_m given in Eq. (7-7) are not constant in time or in space. Moreover, the expressions given by Eq. (7-7) require that the subgrid-scale fluxes be *downgradient* as long as the exchange coefficients are positive. In the atmosphere, *countergradient* turbulent fluxes are often observed (e.g., Deardorff 1966), as discussed just before Section 7.3.3.3. Nonetheless, Eq. (7-7) has been shown to be a useful representation of subgrid-scale fluxes.

Substituting Eq. (7-7) into Eq. (7-6) yields

$$R_f = K_\theta \frac{g}{\theta_0} \frac{\partial \bar{\theta}}{\partial z} \Big/ K_m \left[\left(\frac{\partial \bar{u}}{\partial z} \right)^2 + \left(\frac{\partial \bar{v}}{\partial z} \right)^2 \right]$$

$$= \frac{K_\theta}{K_m} \frac{g}{\theta_0} \frac{\partial \bar{\theta}}{\partial z} \Big/ \left[\left(\frac{\partial \bar{u}}{\partial z} \right)^2 + \left(\frac{\partial \bar{v}}{\partial z} \right)^2 \right] = \frac{K_\theta}{K_m} \text{Ri}, \tag{7-8}$$

where Ri is called the *gradient Richardson number*. The sign of Ri is determined by the sign of the lapse rate of potential temperature. Thus the following conditions apply:

- $\text{Ri} > 0$ corresponds to $\partial \bar{\theta}/\partial z > 0$, which indicates a stably-stratified layer.
- $\text{Ri} = 0$ corresponds to $\partial \bar{\theta}/\partial z = 0$, which corresponds to neutral stratification.
- $\text{Ri} < 0$ corresponds to $\partial \bar{\theta}/\partial z < 0$, which indicates an unstably stratified layer.

Theory (e.g., Dutton 1976:79) indicates that when Ri is greater than 0.25, the stable stratification sufficiently suppresses turbulence so that the flow becomes laminar, even in the presence of mean wind shear. This value of Ri is called the *critical Richardson number*.

The unstable-stratified layer itself is broken down into two regimes:

- $|\text{Ri}| \leq 1$, where the shear production of subgrid-scale kinetic energy is important (a regime referred to as *forced convection*).
- $|\text{Ri}| > 1$, where the shear production becomes unimportant relative to the buoyant product of subgrid-scale kinetic energy (a regime called *free convection*).

The characteristic size of turbulent eddies in the atmosphere are larger during free convection than under forced convection. Brutsaert (1999) provides a recent review of boundary-layer turbulence during free convection.

As reported in Turner (1969), the intensity of turbulence near the ground can be estimated straightforwardly using a wind speed of 10 m, incoming solar radiation, cloud cover, and time of day. The stability classification scheme discussed by Turner forms the foundation of most air quality assessments on the mesoscale in the United States today. Unfortunately, although the dispersion estimates were developed from observations of diffusion over flat, horizontally homogeneous terrain, Gaussian plume models using these estimates are being applied for a wide range of mesoscale systems that are neither flat nor homogeneous. As reported by the American Meteorological Society in a position paper (AMS 1978), over flat, horizontally homogeneous terrain, Gaussian plume models probably give estimates of downwind plume concentrations within a

factor of 2. However, much more serious errors can result when this idealized topography is not achieved (e.g., Pielke *et al.* 1983).

Equation (7-4) can be used to obtain prognostic conservation equations for the subgrid-scale fluxes. Multiplying Eq. (7-4) by u_k'' yields

$$u_k'' \frac{\partial u_i''}{\partial t} = -u_k'' \bar{u}_j \frac{\partial}{\partial x_j} u_i'' - u_k'' u_j'' \frac{\partial u_i''}{\partial x_j} - u_k'' u_j'' \frac{\partial \bar{u}_i}{\partial x_j} + \overline{u_k'' u_j'' \frac{\partial u_i''}{\partial x_j}} - u_k'' \theta_0 \frac{\partial \pi''}{\partial x_i} + g u_k'' \frac{\theta''}{\theta_0} \delta_{i3}. \tag{7-9}$$

Writing Eq. (7-4) with k as the free index and then multiplying by u_i'' yields an equation for $u_i'' \partial u_k''/\partial t$. Adding that equation to Eq. (7-9) results in

$$\frac{\partial}{\partial t}(u_k'' u_i'') = -\bar{u}_j \frac{\partial}{\partial x_j} u_k'' u_i'' - u_j'' \frac{\partial}{\partial x_j} u_k'' u_i'' - u_i'' u_j'' \frac{\partial \bar{u}_k}{\partial x_j} - u_k'' u_j'' \frac{\partial \bar{u}_i}{\partial x_j} + \overline{u_i'' u_j'' \frac{\partial}{\partial x_j} u_k''} + \overline{u_k'' u_j'' \frac{\partial u_i''}{\partial x_j}} - u_i'' \theta_0 \frac{\partial \pi''}{\partial x_k} - u_k'' \theta_0 \frac{\partial \pi''}{\partial x_i} + g u_i'' \frac{\theta''}{\theta_0} \delta_{k3} + g u_k'' \frac{\theta''}{\theta_0} \delta_{i3}. \tag{7-10}$$

Grid-volume averaging Eq. (7-10) using the assumptions given by Eq. (4-8) yields

$$\frac{\partial}{\partial t} \overline{u_k'' u_i''} = -\bar{u}_j \frac{\partial}{\partial x_j} \overline{u_k'' u_i''} - \overline{u_j'' \frac{\partial}{\partial x_j} u_k'' u_i''} - \overline{u_i'' u_j''} \frac{\partial \bar{u}_k}{\partial x_j} - \overline{u_k'' u_j''} \frac{\partial \bar{u}_i}{\partial x_j} - \theta_0 \overline{u_i'' \frac{\partial \pi''}{\partial x_k}} - \theta_0 \overline{u_k'' \frac{\partial \pi''}{\partial x_i}} + \frac{g}{\theta_0} \delta_{k3} \overline{u_i'' \theta''} + \frac{g}{\theta_0} \delta_{i3} \overline{u_k'' \theta''}. \tag{7-11}$$

Prognostic subgrid-scale equations can also be obtained for $\overline{u_i'' \theta''}$, $\overline{u_i'' q_k''}$, and $\overline{u_i'' \chi_m''}$. To illustrate how these equations are derived, multiply Eq. (7-4) by θ'', which results in

$$\theta'' \frac{\partial u_i''}{\partial t} = -\theta'' \bar{u}_j \frac{\partial}{\partial x_j} u_i'' - \theta'' u_j'' \frac{\partial u_i''}{\partial x_j} - \theta'' u_j'' \frac{\partial \bar{u}_i}{\partial x_j} + \theta'' \overline{u_j'' \frac{\partial u_i''}{\partial x_j}} - \theta'' \theta_0 \frac{\partial \pi''}{\partial x_i} + g \frac{\theta''^2}{\theta_0} \delta_{i3}. \tag{7-12}$$

A prognostic equation for θ'' can be obtained in a manner analogous to that used to obtain Eq. (7-4). Equation (2-44) for θ can be written as

$$\frac{\partial}{\partial t}(\bar{\theta} + \theta'') = -(\bar{u}_j + u_j'') \frac{\partial}{\partial x_j}(\bar{\theta} + \theta'') + S_\theta.$$

The source–sink term, S_θ, can be decomposed into a portion that is dependent only on grid-resolved quantities, which are defined here as $\bar{S}_\theta$, and a remainder that is also a function of subgrid-scale effects, S_θ''. Averaging this relation over a grid volume using Eq. (4-6) and applying the assumptions given by Eq. (4-8) yields

$$\frac{\partial \bar{\theta}}{\partial t} = -\bar{u}_j \frac{\partial}{\partial x_j} \bar{\theta} - \overline{u_j'' \frac{\partial \theta''}{\partial x_j}} + \bar{S}_\theta.$$

Note that requiring $\overline{S_\theta''} \equiv 0$ assumes that the source–sink term has subgrid-scale effects that average to 0 across the grid volume. This assumption is likely to be often unrealistic, but nonetheless is used here in the derivation of θ''.

Subtracting the equation for $\frac{\partial \bar{\theta}}{\partial t}$ from $\frac{\partial (\bar{\theta}+\theta'')}{\partial t}$ yields

$$\frac{\partial \theta''}{\partial t} = -\bar{u}_j \frac{\partial \theta''}{\partial x_j} - u_j'' \frac{\partial}{\partial x_j}(\bar{\theta} + \theta'') + \overline{u_j'' \frac{\partial \theta''}{\partial x_j}} + S_\theta - S_\theta''. \tag{7-13}$$

Equation (7-13) can be multiplied by u_i'' and added to Eq. (7-12). Performing the grid-volume average to this equation, using the assumptions given by Eq. (4-8) results in

$$\begin{aligned} \frac{\partial}{\partial t} \overline{u_i'' \theta''} = &-\bar{u}_j \frac{\partial}{\partial x_j} \overline{u_i'' \theta''} - \overline{u_j'' u_i''} \frac{\partial \bar{\theta}}{\partial x_j} - \overline{\theta'' u_j''} \frac{\partial \bar{u}_i}{\partial x_j} - \overline{u_j'' u_i'' \frac{\partial \theta''}{\partial x_j}} \\ &- \overline{\theta'' u_j'' \frac{\partial u_i''}{\partial x_j}} - \theta_0 \overline{\theta'' \frac{\partial \pi''}{\partial x_i}} + \frac{g}{\theta_0} \delta_{i3} \overline{\theta''^2} + \overline{u_i'' S_\theta''}. \end{aligned} \tag{7-14}$$

The prognostic equation for $\overline{\theta''^2}$ can be determined from Eq. (7-13) by multiplying that expression by θ'' and applying the assumption given by Eq. (4-8), which results in

$$\frac{\partial \overline{\theta''^2}}{\partial t} = -\bar{u}_j \frac{\partial}{\partial x_j} \overline{\theta''^2} - \overline{u_j'' \theta''} \frac{\partial}{\partial x_j} \bar{\theta} - \overline{u_j'' \frac{\partial}{\partial x_j} \theta''^2} - \overline{\theta'' S_\theta''}.$$

These prognostic equations for the subgrid-scale fluxes are referred to as *second-order closure equations*, since they provide explicit conservation equations that are part of

- the conservation-of-velocity equation, $\partial(\overline{u_k'' u_i''})/\partial t$,
- the conservation-of-heat equation, $\partial(\overline{u_i'' \theta''})/\partial t$,
- the conservation-of-water equation, $\partial(\overline{u_i'' q''})/\partial t$,
- the conservation-of-other atmospheric gases and aerosols equation, $\partial(\overline{u_i'' \chi_m''})/\partial t$, and
- the conservation-of-mass of air equation, $\partial(\overline{\rho'' u_i''})/\partial t$.

(7-15)

Of these equations, when the assumption that $|\rho''|/\rho_0 \ll 1$ is made, an equation for $\overline{\rho'' u_i''}$ is ignored.

The full equations represented by Eq. (7-15) are computationally expensive to solve, and in all cases either prognostic equations must be developed for the third-order correlation terms (i.e., $\overline{u_j'' \frac{\partial}{\partial x_j} \theta''^2}$, $\overline{u_j'' \frac{\partial}{\partial x_j} u_k'' u_i''}$, etc.) or an assumption made regarding their functional form. The development of prognostic equations will introduce fourth-order correlation terms with an even higher computational cost. The necessity of truncating the derivation of successively higher-order subgrid-scale prognostic equations is called *closure*. Second-order closure, for example, means that functional forms are assumed for the third-order correlation terms. Third-order closure means that functional terms are specified for the fourth-order closure terms that appear in the prognostic equations for the third-order terms.

Mellor and Yamada (1974) present a classic overview of subgrid-scale flux closure schemes. They start with the complete subgrid flux equations such as those shown by, for example, Eqs. (7-11) and (7-14). They then define different levels of complexity in which they discriminate into four levels of detail in the parameterizations. Their level 4, for example, retains the complete subgrid flux equations in their prognostic form, while level 1 is of the form given by Eq. (7-7). Shafran *et al.* (2000) discuss level-1.5 parameterizations in which the only prognostic subgrid flux equation used is the equation for subgrid-scale kinetic energy. In the words of Mellor and Yamada (1974), the goal of developing a hierarchical representation is to obtain a parameterization that is "intuitively attractive and which optimizes computational speed and convenience without unduly sacrificing accuracy." Petersen and Holtslag (1999) discuss, for example, a first-order closure for the fluxes and covariances of χ. Sharan *et al.* (1999) use a level-2 Mellor–Yamada framework to represent σ_w in a stable boundary layer. Glendening (2000) discusses the turbulent kinetic energy budgets for strong shear conditions.

7.2 Surface Layer Parameterization

A parameterization of the vertical subgrid-scale fluxes near the ground can be obtained using relations such as those given by Eq. (7-7), along with the requirement of dimensional consistency.[7] This parameterization plays a major role in the parameterization of the planetary boundary layer as discussed later in this chapter.

From Eq. (7-7),

$$\overline{w''u''} = -K_m \frac{\partial \bar{u}}{\partial z} = -u_*^2 \cos\mu$$
$$\overline{w''v''} = -K_m \frac{\partial \bar{v}}{\partial z} = -u_*^2 \sin\mu, \tag{7-16}$$

with

$$\arctan(\bar{v}/\bar{u}) = \mu \qquad \text{and} \qquad \bar{\rho} u_*^2 = \tau.$$

Equation (7-16) is a level-1 representation. The parameter u_* is called the *friction velocity*,[8] which, when squared and multiplied by the fractional contribution of the mean wind to each component direction, is equal to the subgrid-scale fluxes on the left side of Eq. (7-16). The variable τ is the *shearing stress* caused by the horizontal wind. If $\overline{V}$ is the magnitude of the grid-volume–averaged flow $[\overline{V} = (\bar{u}^2 + \bar{v}^2)^{1/2}]$, then Eq. (7-16) can also be written as

$$K_m \, \partial \overline{V}/\partial z = u_*^2. \tag{7-17}$$

Since K_m has dimensions of a length multiplied by a velocity, it is reasonable to assume that

$$K_m = kzu_*. \tag{7-18}$$

In Eq. (7-16), the friction velocity is the characteristic velocity and kz is used as a length scale of turbulent eddies near the ground. The constant of proportionality, k, is called *von Karman's constant*, which from observations in the atmosphere (e.g., Högström 1996) is estimated to have a value of $k = 0.40 \pm 0.01$ (although Bergmann 1998 reports on a value of $k = 0.3678$; discussions of this value of the von Karman constant are given in Andreas and Treviño 2000 and Bergmann 2000). The relation given by Eq. (7-18), however, only applies when buoyancy production of turbulent kinetic energy is negligible (i.e., $\mathrm{Ri} \simeq 0$), with the shear of the mean wind providing the source for the turbulent energy.

Substituting Eq. (7-18) into (7-17) yields

$$\partial \overline{V}/\partial z = u_*/kz, \tag{7-19}$$

which, integrating between the level $\overline{V} = 0$ (defined as z_0) and an arbitrary level above the ground z, gives

$$\int_{z_0}^{z} \frac{\partial \overline{V}}{\partial z} \, dz = \overline{V}(z) = \int_{z_0}^{z} \frac{u_*}{kz} \, dz = \frac{u_{*_0}}{k} \int_{z_0}^{z} \frac{dz}{z} = \frac{u_{*_0}}{k} \ln \frac{z}{z_0}. \tag{7-20}$$

This relation is called the *logarithmic wind profile*, and z_0 is called the *aerodynamic roughness*. With relatively homogeneous upwind fetch, Carl *et al.* (1973) found no significant deviation of the wind profile from Eq. (7-20) up to 150 m when |Ri|, as computed from data at 18 and 30 m on a tower, was

less than 0.05. In performing the integration in Eq. (7-20), u_* was assumed to be invariant with height; thus the layer over which Eq. (7-20) is an accurate approximation is often called the *constant flux layer*. This term is inaccurate, however, since the flux usually decreases exponentially near the surface. If the surface layer were associated with a constant flux, then the wind speeds could not decrease near the surface, since $\frac{\partial}{\partial z} u_*^2 = \frac{\partial}{\partial z} \overline{V''w''}$ would be 0! It is more appropriate to define u_* as the layer-averaged value using the mean-value theorem of calculus to factor u_* through the integral in Eq. (7-20). This is the reason why the subscript "0" was included in u_* in Eq. (7-20). In addition, the wind is assumed to not change direction with height; otherwise, Eq. (7-20) could not be written as a scalar equation.

The value of z_0 depends on the characteristics of the surface, ranging from a value of 0.001 cm over smooth ice to 10 m over large buildings (Oke 1978). Driese and Reiners (1997) provide values of z_0 for semi-arid natural shrubland. Over some surfaces, such as long grasses and water, z_0 can be a function of the friction velocity. Over sand, for example, as reported by Bagnold (1973), and Vugts and Cannemeijer (1981), z_0 increases substantially when $u_* \geq 0.1(\rho_s \bar{\rho}^{-1} g d)^{1/2}$, because of the aeolian transport of sand at stronger wind speeds. In this expression, ρ_s is the density of sand and d is the diameter of the sand grains, assuming that all are of the same size.

Over water, Garratt (1992) suggested the form

$$z_0 = (0.01625 \pm 0.00225) u_*^2 / g, \tag{7-21}$$

while Sheih *et al.* (1979) suggested the form

$$z_0 = \left(0.016 u_*^2 / g\right) + v/(9.1 u_*),$$

where v is the kinematic viscosity of air ($\sim 1.5 \times 10^{-5}$ s^{-1}). Additional discussion of values of z_0 to use over water, including the effect of waves, is given in Powers and Stoelinga (2000). The modification of surface drag by ocean waves is discussed in Donelan *et al.* (1997). Zeng *et al.* (1998) also summarize forms of z_0 to use over water. Chamberlain (1983) suggested that Eq. (7-21) may also apply over other mobile surfaces, such as sand and snow.

Representative values of z_0 are presented in Table 7-2. A useful illustration of characteristic values of roughness is given in McRae *et al.* (1982a, Figure 3). The paper by van Dop (1983) provides a map of estimated average values of z_0 for areas on the order of 20×20 km^2 in the Netherlands based on several land-type categories.

For specific locations, z_0 is calculated by taking wind observations at several heights within the surface layer when the mean wind speed is strong, so that Ri = 0 and $\overline{V} \simeq (u_*/k) \ln(z/z_0)$ from Eq. (7-20) can be used. The winds are then plotted as a function of the natural logarithm of height, as illustrated in Figure 7-2 and extrapolated to the value $\overline{V} = 0$. The intersection of the ln z-axis

TABLE 7-2.

Representative Values of Aerodynamic Roughness for a Uniform Distribution of These Types of Ground Cover.

	Aerodynamic roughness, z_0	Height of of ground cover	Displacement height, D
Ice[a]	0.001 cm		
Smooth mud flats[f]	0.001 cm		
Snow[a]	0.005–0.01 cm		
Sand[a]	0.03 cm		
Smooth desert[f]	0.03 cm		
Smooth snow on short grass [c]	0.005 cm		
Snow surface, natural prairie[c]	0.1 cm		
Soils[a]	0.1–1 cm		
Short grass[a]	0.3–1 cm	2–10 cm	
Mown grass[c]	0.2 cm	1.5 cm	
	0.7 cm	3 cm	
	2.4 cm with $\overline{V}$ at 2 m = 2 m s^{-1}	4.5 cm	
	1.7 cm with $\overline{V}$ at 2 m = 6.8 m s^{-1}		
Long grass[a]	4–10 cm	25 cm–1 m	
Long grass (60–70 cm)	15 cm[f], 9 cm[c] with $\overline{V}$ at 2 m = 1.5 m s^{-1}		
	11 cm[f], 6.1 cm[c] with $\overline{V}$ at 2 m = 3.5 m s^{-1}		
	8 cm[f], 3.7 cm[c] with $\overline{V}$ at 2 m = 6.2 m s^{-1}		
Agricultural crops[a]	4–20 cm[d]	~40 cm–2 m[d]	~27–~1.3 m[e]
Orchards[a]	50–1 m[d]	~5 m–10 m[d]	~3.3–~6.7 m[e]
Deciduous forests[a]	1–6 m[d]	~10 m–60 m[d]	~6.7–~40 m[e]
Coniferous forests[a]	1–6 m[d]	~10 m–60 m[d]	~6.7–~40 m[e]
Rural Delmarva peninsula[b]	33 cm (for NW flow)		
Pakistan desert[c]	0.03 cm		

[a] From Oke (1978).
[b] From Snow (1981).
[c] From Priestly (1959).
[d] Using Eq. (7-36).
[e] Using Eq. (7-35).
[f] From Sellers (1965).

defines z_0. For particularly complex locations, such as city centers, Davenport *et al.* (2000) recommends determining effective roughness using scale models in wind tunnels.

When the atmosphere near the ground is not neutrally stratified, Eq. (7-19) must be generalized to include buoyancy effects. The flux Richardson number

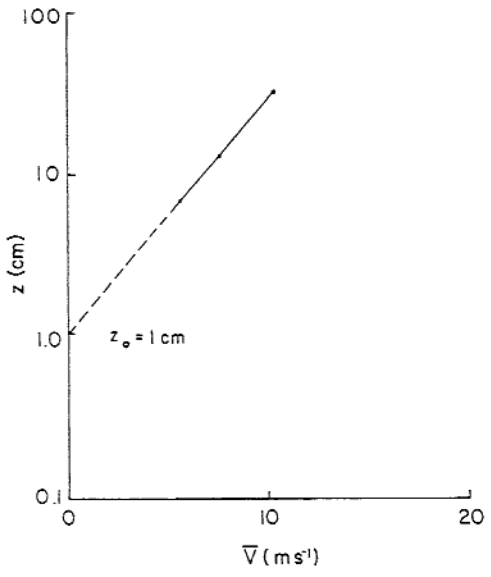

Fig. 7-2. Schematic illustration of the procedure used to compute z_0 from observations of mean wind speed at three levels near the ground in a neutrally stratified atmosphere. The slope of the line gives k/u_*.

given by Eq. (7-6) can be written as

$$R_f = \frac{-g}{\theta_0} \overline{w''\theta''} \Big/ u_*^2 \frac{\partial \overline{V}}{\partial z}, \tag{7-22}$$

using Eq. (7-16) and the definition of $\overline{V}$.[9] The flux Richardson number is then multiplied by

$$\phi_M = \frac{kz}{u_*} \frac{\partial \overline{V}}{\partial z}, \tag{7-23}$$

where ϕ_M is called the *nondimensional wind shear*, yielding

$$R_f \phi_M = -g \overline{w''\theta''} kz/\theta_0 u_*^3 = z/L. \tag{7-24}$$

The value of ϕ_M is defined as unity under neutral stratification [so that Eq. (7-19) is satisfied] and as a function of the flux Richardson number otherwise. The parameter $L = -\theta_0 u_*^3/g\overline{w''\theta''} k$ has the dimensions of a length and is called the *Monin length*. Since ϕ_M is assumed to be a function of R_f, ϕ_M can be written as

$$\phi_M = \phi_M(R_f) = \phi_M(\phi_M R_f/\phi_M) = \phi_M\big((z/L)\phi_M\big) = \phi_M(z/L)$$

using Eq. (7-24), so that ϕ_M is a function of z/L only. Values of ϕ_M determined from observations are given in Figure 7-3. When $z/L < 0$ (the atmosphere

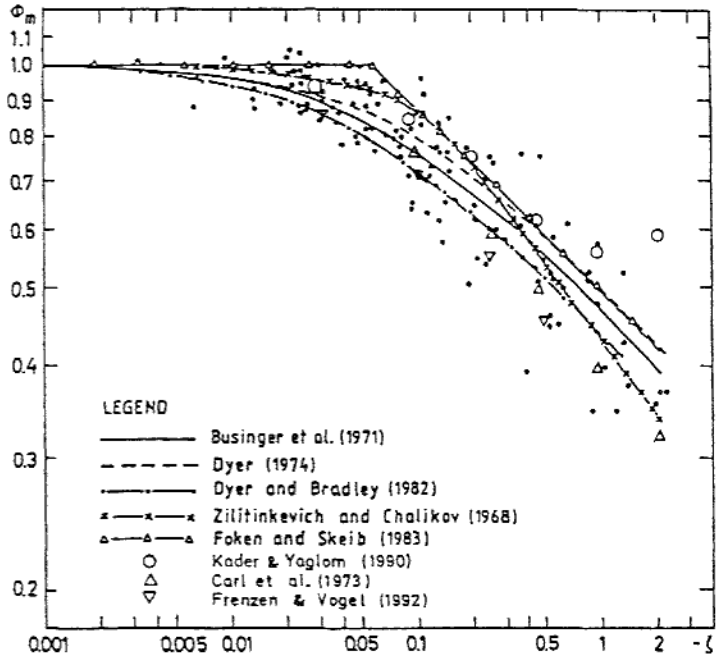

Fig. 7-3. Plot of ϕ_M against $(z - d)/L$ in log-log representation for unstable stratification. The small dots are data from Högström (1988). The other symbols have been derived from modified expressions from the sources listed in the key. (From Högström 1996 with kind permission from Kluwer Academic Publishers.)

is unstably stratified), $\phi_M < 1$, while under a stable stratification, $\phi_M > 1$. The modification to the wind profile can be determined using Eq. (7-23) and Figure 7-3. The definition given by Eq. (7-23) can be rewritten as

$$\frac{kz}{u_*}\frac{\partial \overline{V}}{\partial z} = 1 - (1 - \phi_M),$$

or

$$\frac{\partial \overline{V}}{\partial z} = \frac{u_*}{kz} - \frac{(1 - \phi_M)}{kz}u_*. \tag{7-25}$$

Integrating Eq. (7-25) with height, as was performed to achieve Eq. (7-20), gives

$$\overline{V} = \frac{u_{*_0}}{k}\ln\frac{z}{z_0} - \frac{u_{*_0}}{k}\int_{z_0/L}^{z/L}(1 - \phi_M)d\ln\frac{z}{L}, \tag{7-26}$$

where a change of variable was made in the integrand and limits. In writing the right side of Eq. (7-26), L_0 and u_{*_0} are assumed to be constant with height

(L_0 is the layer-averaged value of the Monin length, L). Equation (7-26) is often written in the form

$$\overline{V}(z) = \frac{u_*}{k}\left[\ln\frac{z}{z_0} - \psi_M\left(\frac{z}{L}\right)\right], \tag{7-27}$$

where $z/L \gg z_0/L$ is assumed; that is,

$$\psi_M = \int_0^{z/L} \frac{(1-\phi_M)}{z/L}\, d\left(\frac{z}{L}\right). \tag{7-28}$$

The function $\psi_M(z/L)$ is the correction to the logarithmic wind profile resulting from the deviation from neutral stratification. For a neutral stratification, $\psi_M = 0$. Figure 7-4 schematically illustrates the form of $\overline{V}$ when plotted as a function of ln z for stable, unstable, and neutral stratification. Note that z_0 is presumed to be independent of stability, so that each profile is extrapolated to the same value. This is required since ϕ_M approaches unity as z decreases (i.e., $z/L = z_0/L \simeq 0$ if $z_0 \ll L$). Specific observational estimates of ϕ_M are discussed in Högström (1996), with one suggested formula presented in Eq. (7-42).

Expressions analogous to ϕ_M and ψ_M can also be derived for the vertical subgrid-scale fluxes of potential temperature, water, and other gaseous and

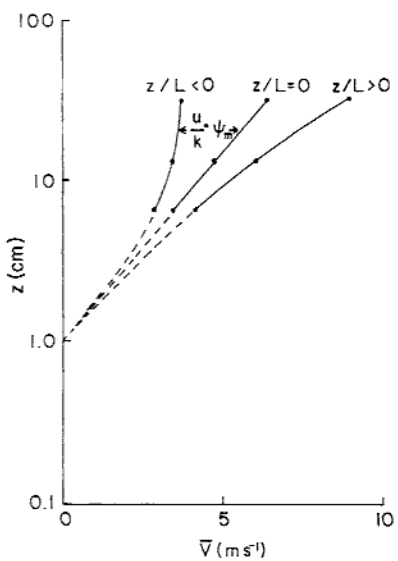

Fig. 7-4. Schematic illustration of the procedure used to compute the wind profile near the ground from observations of mean wind speed at three levels, along with the knowledge of the stability as measured by z/L. The difference between the logarithmic wind profile and the actual wind profile at any level is given by $(u_*/k)\,\psi_M$ [from Eq. (7-27); $\psi_M < 0$ when $z/L > 0$, $\psi_M > 0$ when $z/L < 0$].

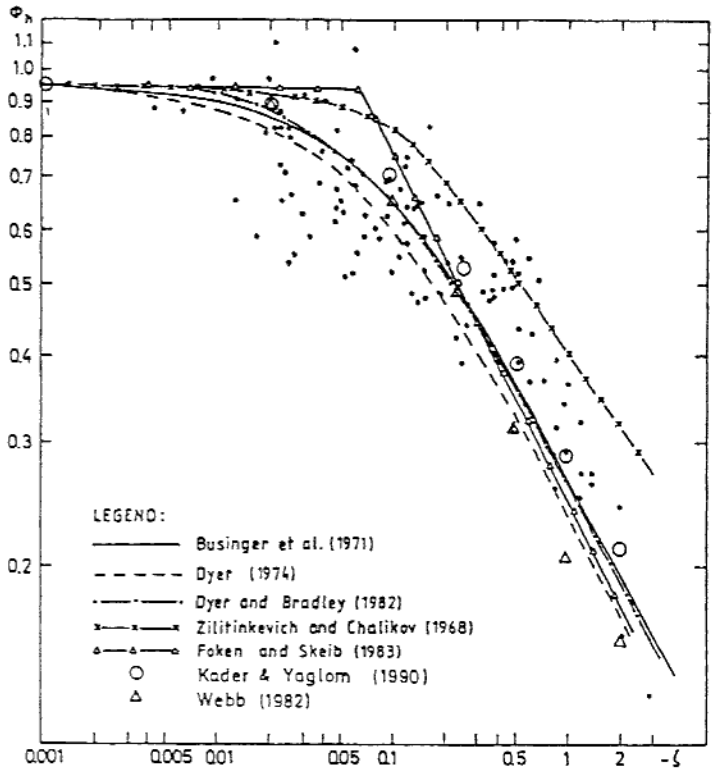

Fig. 7-5. As in Figure 7-3 except for ϕ_H. (From Högström 1996 with kind permission from Kluwer Academic Publishers.)

aerosol atmospheric materials. Figure 7-5 illustrates a function form for ϕ_H. From Eq. (7-7), and using the same form to represent $\overline{w''q_n''}$ and $\overline{w''\chi_m''}$,

$$\overline{w''\theta''} = -K_\theta \frac{\partial \bar{\theta}}{\partial z} = -u_* \theta_*,$$

$$\overline{w''q_n''} = -K_q \frac{\partial \bar{q}_n}{\partial z} = -u_* q_{n_*}, \tag{7-29}$$

$$\overline{w''\chi_m''} = -K_\chi \frac{\partial \overline{\chi}_m}{\partial z} = -u_* \chi_{m_*}.$$

The parameter θ_* could be called the *flux temperature*, and q_{n_*} and χ_{m_*} are similar variables that have not been assigned labels. Generally, K_q and K_χ are assumed to be equal to K_θ (Yamada 1977), since within the surface layer, θ, q_n, and χ_m are presumed to mix solely by subgrid-scale advection. The value of K_m, in contrast, also includes the effect of the subgrid-scale pressure on the subgrid-scale velocity [as is evident from, for example, Eq. (7-4)], so that in

general, K_m is not assumed to be equal to the other three exchange coefficients. Warhaft (1976) also shows that there should be differences between K_θ and K_{q_3} when the correlation $\overline{\theta'' q_3''}$ is small or when $\partial\bar{\theta}/\partial z$ and $\partial\bar{q}/\partial z$ have opposite signs. However, these effects are expected to have a relatively small effect on the magnitude of the exchange coefficients (Wyngaard 1981, personal communication), although Lang *et al.* (1983) presented evidence that K_θ and K_{q_3} can be significantly different when substantial horizontal advection of heat and moisture occur over a cool surface. Nevertheless, in the analysis presented below, an equality between K_θ and K_{q_3} is assumed, which should be valid except over wet areas surrounded by warmer, dry land. This topic requires additional study.

By analogy with Eq. (7-23),

$$\frac{\beta k z}{\theta_*}\frac{\partial\bar{\theta}}{\partial z} = \frac{\beta k z}{q_{n_*}}\frac{\partial\bar{q}_n}{\partial z} = \frac{\beta k z}{\chi_{m_*}}\frac{\partial\overline{\chi}_m}{\partial z} = \beta\phi_{\mathrm{H}} = \hat{\phi}_{\mathrm{H}}, \tag{7-30}$$

where the scale and intensity of turbulent mixing of $\bar{\theta}$, $\bar{q}_n$, and $\overline{\chi}_m$ are assumed to be the same, with β used to indicate that the characteristic vertical mixing length for $\bar{\theta}$, $\bar{q}$, and $\overline{\chi}_m$ can be different than that for $\overline{V}$. It has also been shown that radiative cooling can significantly affect the magnitude of ϕ_{H} (Garratt and Brost 1981; Gopalakrishnan *et al.* 1998). In Eq. (7-30), $\hat{\phi}_{\mathrm{H}}$ equal to unity at $z/L = 0$ is required.

Following the same procedure as that used to derive Eq. (7-25) yields

$$\begin{aligned}
\bar{\theta}(z) &= \bar{\theta}(z_0) + \frac{\theta_*}{\beta k}\left[\ln\frac{z}{z_0} - \psi_{\mathrm{H}}\left(\frac{z}{L}\right)\right],\\
\bar{q}_n(z) &= \bar{q}_n(z_0) + \frac{q_{n_*}}{\beta k}\left[\ln\frac{z}{z_0} - \psi_{\mathrm{H}}\left(\frac{z}{L}\right)\right],\\
\overline{\chi}(z) &= \overline{\chi}_m(z_0) + \frac{\chi_{m_*}}{\beta k}\left[\ln\frac{z}{z_0} - \psi_{\mathrm{H}}\left(\frac{z}{L}\right)\right],
\end{aligned} \tag{7-31}$$

where

$$\psi_{\mathrm{H}} = \int_0^{z/L}\frac{1-\hat{\phi}_{\mathrm{H}}}{z/L}\,d(z/L), \tag{7-32}$$

with a plot of ϕ_{H} as a function of z/L from Högström (1996) given in Figure 7-5. In the derivation of ψ_{H}, $z_0 \ll z$ has been assumed. The first terms on the right side of each equation in Eq. (7-31) are the values of $\bar{\theta}$, $\bar{q}_n$, and $\overline{\chi}_m$ evaluated at the level where $\overline{V}$ becomes 0 (i.e., z_0), although some conclude that a different roughness length should be used (see Mahrt 1996:95–96 for a discussion; also Bosveld *et al.* 1999, Junfang *et al.* 1999, and Ren *et al.* 1999). Ma and Daggupaty (1998) discuss effective roughness lengths of momentum and heat exchange associated with roughness changes. Sun (1999) concluded

that it is more accurate to define $\theta(z_0)$ in terms of the surface irradiance temperature rather than using the surface radiation temperature and adjusting a z_0 specifically for θ. She also found that a roughness length defined for θ varies in space and time much more than z_0 as obtained from Eq. (7-20). Hence in this chapter we use the same z_0 for Eq. (7-31).

Substituting from Eqs. (7-30) and (7-23) for the vertical gradient terms in Eqs. (7-29) and (7-17) gives

$$K_m = \frac{ku_* z}{\phi_M} \quad \text{and} \quad K_\theta = \frac{\beta k u_* z}{\hat{\phi}_H}, \tag{7-33}$$

which provides estimates of the exchange coefficients near the ground.

The relation between K_θ and K_m can be derived for certain circumstances. Pandolfo (1966) has shown from observations that $z/L = \text{Ri}$ near the ground under neutral and unstably stratified lapse rates. When this is true,

$$\text{Ri} = z/L = \phi_M R_f = \phi_M (K_\theta / K_m)\text{Ri},$$

from Eqs. (7-24) and (7-8), so that $K_m/K_\theta = \phi_M$. Therefore, from Eq. (7-33),

$$K_\theta = ku_* z/\phi_M^2.$$

Thus, since $\phi_M < 1$ when $z/L < 0$ (see, e.g., Figure 7-3), the turbulent mixing of $\bar{\theta}$, $\bar{q}_n$, and $\overline{\chi}_m$ is greater than that for velocity in unstable air near the ground. Unfortunately, this result is not consistent with a value of β different than 1. From this analysis, $K_m = K_\theta$ when $z/L = 0$, since ϕ_M for that value is unity. However, from Eq. (7-33) and Figs. 7-3 and 7-5, $K_\theta \simeq 1.05\, K_m$ at $z/L = 0$. Reexamination of the data is needed to clear up this discrepancy near $z/L = 0$. However, the values of K_m and K_H are closer to each other at $z/L = 0$ using the Högström (1996) paper than in the earlier Businger *et al.* (1971) formulation summarized in Pielke (1982).

When the ground cover is sufficiently high so that significant turbulent flow can occur below the top (e.g., within a pine forest, cornfield, etc.), Eqs. (7-27) and (7-31) must be rewritten as

$$\left.\begin{aligned}
\overline{V}(\bar{z}) &= \frac{u_*}{k}\left[\ln\frac{z-D}{z_0} - \psi_M\left(\frac{z-D}{L}\right)\right] \\
\bar{\theta}(z) &= \bar{\theta}_0(D+z_0) + \frac{\theta_*}{\beta k}\left[\ln\frac{z-D}{z_0} - \psi_H\left(\frac{z-D}{L}\right)\right] \\
\bar{q}_n(z) &= \bar{q}_{n_0}(D+z_0) + \frac{q_{n_*}}{\beta k}\left[\ln\frac{z-D}{z_0} - \psi_H\left(\frac{z-D}{L}\right)\right] \\
\overline{\chi}_m(z) &= \overline{\chi}_{m_0}(D+z_0) + \frac{\chi_{m_*}}{\beta k}\left[\ln\frac{z-D}{z_0} - \psi_H\left(\frac{z-D}{L}\right)\right]
\end{aligned}\right\} z \geq D+z_0, \tag{7-34}$$

where D is called the *zero-plane displacement.*[10] Values of z_0 used in these relations are displaced a distance D from the actual ground surface. In other words, because of the significant height of ground cover, $\overline{V}$, $\bar{\theta}$, $\bar{q}_n$, and χ_m respond to the aerodynamic roughness of the top of the ground cover (e.g., the canopy) rather than the ground surface or the morphology within the high ground cover. To be a realistic representation of the ground cover, however, the cover must be uniformly distributed, such as in a forest or large agricultural area. The values of $\bar{\theta}(D + z_0)$, $\bar{q}_{n_0}(D + z_0)$, and $\overline{\chi}_{m_0}(D + z_0)$ are the values that would occur if the height $z = D$ actually corresponded to $z \simeq 0$. Similarly, $\overline{V}(D + z_0)$ would equal 0 if $z = D$ actually were $z \simeq 0$, as shown schematically by the dashed line in Figure 7-6.

Values of D are determined experimentally by plotting wind speed as a function of $\ln(z - D)$ for strong winds. Different D values are substituted into the expression for $\overline{V}$ given in Eq. (7-34) until the logarithmic wind profile is achieved (i.e., a straight line, as illustrated schematically in Figure 7-7).

A useful formula to estimate D for closely spaced stands of crops and trees (from Oke 1978:98) is given by

$$D = \frac{2}{3}h, \tag{7-35}$$

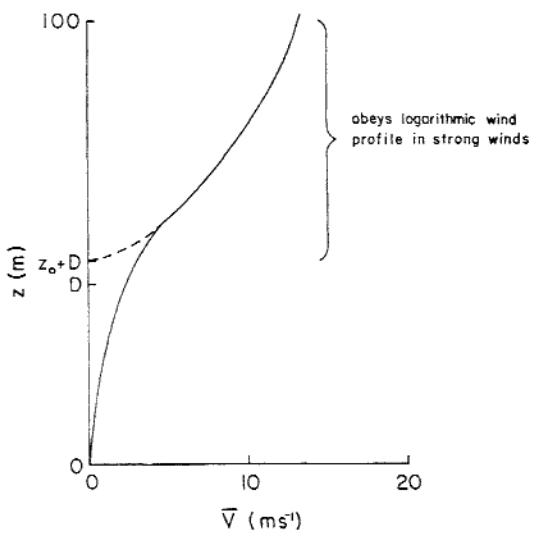

Fig. 7-6. Schematic illustration of a wind profile (solid line) above and within a dense, horizontally and vertically uniform ground cover. The dashed line represents the expected wind profile if $D = 0$. Below $z_0 + D$, the profile obeys Eq. (7-37) with a constant value of a.

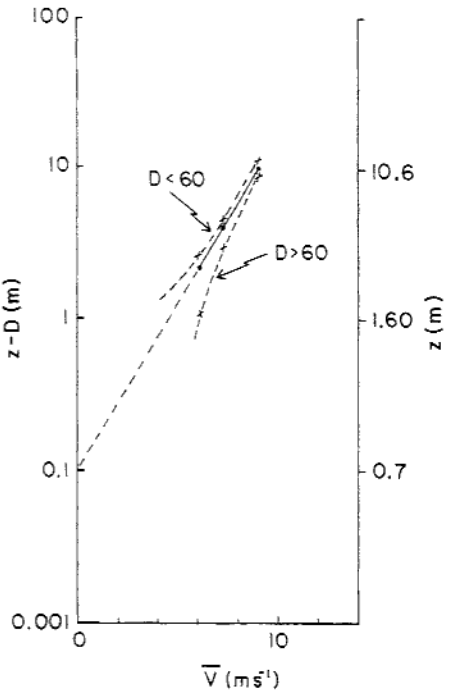

Fig. 7-7. Schematic illustration of the procedure used to compute the wind profile over tall, dense ground cover given three wind observations over the cover and Ri $\simeq$ 0. In this example, $D = 60$ cm is assumed to give the best fit to the logarithmic wind profile; z_0 is then determined to equal 10 cm.

where h is the height of the vegetation. Oke (1978:119) also reports on a suggested relationship between roughness and vegetation height for tall, dense vegetation, which is given by

$$\log_{10} z_0 = \log_{10} h - 0.98, \tag{7-36}$$

so that $z_0 \simeq h/10$. Rosenberg (1974) reports on a formulation for D, based on observations over different types of agricultural crops given by

$$\log_{10} D = 0.979 \log_{10} h - 0.154.$$

Within the ground cover, a wind profile of

$$\overline{V} = \overline{V}_D \exp a \left(\frac{\ln z}{\ln D} - 1 \right) \qquad (a > 0) \tag{7-37}$$

can be assumed, with $\overline{V} = \overline{V}_D$ at the zero-plane displacement height and $\lim_{z \to 0} \overline{V} \to 0$.[11] However, this expression is accurate only when the density of

the ground cover is uniform with height. In a non-uniformly distributed ground cover, such as a deciduous forest, a local wind maximum can occur below the leaf canopy in the trunk region. Monteith (1975b) provides details on wind profiles (and vertical distributions of other variables) in a variety of vegetation types. When Eq. (7-37) is used within a vegetative cover, a is assumed to be directly proportional to the *leaf area index* L_A, where

$$L_A = A_S/A_G, \tag{7-38}$$

with A_S the total leaf area per area of ground surface A_G.

The value of a in Eq. (7-37) is experimentally determined by plotting observed wind speeds in the form of $\ln(\overline{V}/\overline{V}_D)$ within the ground cover as a function of $(\ln z/ln\, D) - 1$. Fitting the data with a straight line, and recognizing that $\overline{V} = 0$ at $z = 0$, yields a. Within corn, for example, Blackadar (1969, personal communication) estimates a value of $a \simeq 2.0$ using the relationship $\overline{V} = \overline{V}_D \exp a[(z/D) - 1]$.

In his simulation of drainage flow, Garrett (1983a) also found that wind speeds are substantially influenced by the presence of forest. With a 50% coverage of forest, his model predicts a 50% decrease in maximum velocity and depth of the nocturnal drainage flow. Yamada's (1982) model of the boundary layer structure over flat terrain simulates nearly constant low wind speeds within a forest canopy with large wind shears near the treetops. Oke (1978:131) concluded that for a given wind speed, the atmosphere is more turbulent over a forest than over any other natural surface (excluding topographic effects). Wilson and Shaw (1977) have presented results using a second-order–closure, one-dimensional model of the flow within a corn crop. Lord *et al.* (1972) used a one-dimensional model to investigate the effect of tundra vegetation on the land-air interface and concluded that a three-dimensional representation is necessary to account for the horizontal heterogeneity caused by the presence of thaw lakes atop the permafrost.

Figure 7-6 illustrates how a wind profile would appear during neutral stratification above and within a dense, horizontally and vertically uniform ground cover when Eqs. (7-34) and (7-37) apply. The profiles of $\tilde{\theta}(z)$, $\tilde{q}_n(z)$, and $\overline{\chi}_m(z)$ within such ground cover are generally more complex, however, since $\tilde{\theta}(z)$ is significantly influenced by radiative flux divergence, whereas water and other gaseous and aerosol atmospheric materials flow into and out of the soil and vegetation. The radiation and moisture budgets within and above vegetation are discussed in Section 11.3.3.2.

Enough basic material has been introduced to permit the discussion of the parameterization of the planetary boundary layer within mesoscale models. Additional discussion of similarity theory can be found in such sources as Jensen and Busch (1982), Arya (1988), Stull (1988), Sorbjan (1989), and Garratt (1992).

7.3 Planetary Boundary-Layer Parameterization

Representation of the planetary boundary layer in mesoscale models is handled primarily through the subgrid-scale correlation terms, since the model grid resolution is too large to resolve explicitly the small-scale fluxes found in this layer. Treatment of the influence of the planetary boundary layer in numerical models can be grouped into two classes:

- those that treat it as a single layer (e.g., Deardorff 1972; Mahrt 1974; Smith and Mahrt 1981)
- those that resolve it into a number of discrete levels.

In mesoscale models, the second approach is the most common. As shown by Anthes *et al.* (1980), for example, detailed boundary-layer resolution is essential for accurate solutions when differential heating along complex terrain and across land–water boundaries is being represented, since significant vertical gradients of the meteorological variables occur within the planetary boundary layer.

With the discrete level approach, the planetary boundary layer can be divided into three sections: viscous sublayer, surface layer, and transition layer.

7.3.1 Viscous Sublayer

The viscous sublayer[12] is defined as the level near the ground ($z < z_0$; with $D \simeq 0$), where the transfer of the dependent variables by molecular motions become important. Zilitinkevich (1970) and Deardorff (1974a) suggest relating temperature and specific humidity at the top of the layer $\bar{\theta}_{z_0}$ and $\bar{q}_{z_0}$ to the surface values of the variables $\bar{\theta}_G$ and $\bar{q}_G$ using expressions of the form

$$\bar{\theta}_{z_0} = \theta_G + 0.0962(\theta_*/k)(u_* z_0/v)^{0.45}$$

and

$$\bar{q}_{z_0} = q_G + 0.0962(q_*/k)(u_* z_0/v)^{0.45}. \tag{7-39}$$

By analogy,

$$\overline{\chi}_{z_0} = \chi_G + 0.0962(\chi_*/k)(u_* z_0/v)^{0.45}.$$

In these expressions, v is the kinematic viscosity of air ($\sim 1.5 \times 10^{-5}$ m^2 s^{-1}) and k is von Karman's constant with θ_*, u_*, q_*, and χ_* defined by Eqs. (7-27) and (7-31). Between $z = z_0$ and $z = z_G$, $\bar{u} = \bar{v} = \bar{w} = 0$, whereas variations of $\bar{p}$ and $\bar{\pi}$ across this depth are ignored.

As discussed by Businger (1973), $u_* z_0/v$ may be considered the Reynolds number of the smallest turbulent eddy in the flow. Businger also reports on a study by Nikuradse (1933) in which laminar flow occurs with $u_* z_0/v < 0.13$,

whereas turbulent motion dominates with $u_* z_0/v > 2.5$. In between these two limits, a transition regime exists. The laminar situation is said to be *aerodynamically smooth*, whereas the fully turbulent flow is *aerodynamically rough*.

7.3.2 Surface Layer

The surface layer extends from z_0 to h_s, with h_s (the top of the surface layer) usually varying from about 10 m to about 100 m. In this layer, the subgrid-scale fluxes are represented by mean-layer values that are assumed to be independent of height and where the veering of the wind with height owing to the Coriolis effect is neglected, as used to derive Eqs. (7-27) and (7-32). With the assumption that the conditions in this layer are steady and horizontally homogeneous, investigators (e.g., Yamamoto 1959; Yamamoto and Shimanuki 1966; Shimanuki 1969) have developed empirical formulations for Eqs. (7-23), (7-28), (7-30), and (7-32), to specify the relationship between the dependent variables and the subgrid-scale fluxes. Högström (1996) provides a recent summary of these formulations. Only a limited number of studies with nonhomogeneous terrain have been done (e.g., Peterson 1969; Taylor 1977a, b; Taylor and Gent 1981) or sloping terrain (e.g., Gutman and Melgarejo 1981), and this work has yet to be applied to mesoscale models.

One of the most common formulations for Eqs. (7-27) and (7-31) used in mesoscale models is that reported by Högström (1996) and Högström (2000, personal communication), in which[13]

$$\begin{aligned} u_{*_0} &= k\overline{V}/\left[\ln(z/z_0) - \psi_{\mathrm{M}}(z/L)\right], \\ \theta_{*_0} &= k\left(\bar{\theta}(z) - \bar{\theta}_{z_0}\right)/0.95\left[\ln(z/z_0) - \psi_{\mathrm{H}}(z/L)\right], \\ q_{*_0} &= k\left(\bar{q}_3(z) - \bar{q}_{z_0}\right)/0.95\left[\ln(z/z_0) - \psi_{\mathrm{H}}(z/L)\right], \\ \chi_{*_{m0}} &= k\left(\overline{\chi}_m(z) - \overline{\chi}_{z_{0_m}}\right)/0.95\left[\ln(z/z_0) - \psi_{\mathrm{H}}(z/L)\right], \end{aligned} \tag{7-40}$$

where

$$\psi_{\mathrm{M}} = \begin{cases} 2\ln\left[(1+\zeta)/2\right] + \ln\left[1+(\zeta^2/2)\right] - 2\tan^{-1}\zeta + \pi/2, & z/L \le 0 \\ -5.3\zeta, \quad 0 < z/L \le 0.5, \\ \quad \text{where } \zeta = (1-19z/L)^{1/4}, \end{cases}$$

$$\psi_{\mathrm{H}} = \begin{cases} 2\ln\left[(1+\zeta_{\mathrm{H}}^2)/2\right], & z/L \le 0 \\ -8.0\zeta, & 0 < z/L \le 0.5, \\ \quad \text{where } \zeta_{\mathrm{H}} = (1-11.6z/L)^{1/4}. \end{cases} \tag{7-41}$$

Högström (2000, personal communication) found that his experimental data for $z/L > 0.5$ show that ϕ_H and ϕ_M tend to level off, but the data are very scattered:

$$\phi_M = \frac{kz}{u_{*_0}}\frac{\partial \overline{V}}{\partial z} \simeq \begin{cases} (1-19z/L)^{-1/4}, & z/L \le 0 \\ 1+5.3z/L, & 0.5 > z/L > 0 \end{cases}$$
$$\phi_H = \frac{kz}{\theta_{*_0}}\frac{\partial \bar{\theta}}{\partial z} = \frac{kz}{q_{*_0}}\frac{\partial \bar{q}_3}{\partial z} = \frac{kz}{\chi_{*_{m_0}}}\frac{\partial \overline{\chi}_m}{\partial z} \simeq \begin{cases} (1-11.6z/L)^{-1/2}, & z/L \le 0 \\ 1+8.0z/L, & 0 \le z/L \le 0.5, \end{cases} \tag{7-42}$$

with the definition of L given in Eq. (7-24), written as $L = \bar{\theta}u_{*_0}^2/kg\theta_{*_0}$. The value of β in Eq. (7-31) was determined to be 1.05. The accuracy of ϕ_M is estimated as 10–20% for unstably stratified surface layers with z/L greater than -0.5. The same accuracy is assumed for ϕ_H for unstably stratified surface layers with z/L greater than -2.0 (Högström 1988). Alternative formulas for these parameters have been suggested by, for example, Viswanadham and Nogueira (1982), who provided estimates of ϕ_M for very stable, unstable, and near-neutral surface-layer stability conditions. Carl *et al.* (1973), using tower data over homogeneous terrain, concluded that ϕ_M approaches a $(-z/L)^{-1/2}$ relationship in an unstably stratified surface layer with $|z/L|$ large, rather than $(-z/L)^{-1/4}$, as given in Eq. (7-42). DeBruin (1999) proposes a formulation for ϕ_M which is a function of $(-z/L)^{-1/3}$ as $(-z/L)$ becomes large and approaches the free convection limit. Hsu *et al.* (1999) propose $\psi_M(z/L) = a(-z/L)^b$, with $a = 1.0496$ and $b = 0.4591$ for $z/L < 0$. However, these refinements to ϕ_M and ϕ_H as applied to mesoscale modeling are relatively minor and should have only a small effect on the resultant mean profiles of the dependent variables.

The subgrid-scale flux of other gaseous and atmospheric materials can also be written as

$$\overline{w''\chi_m''} = -v_s\overline{\chi}_{m_z},$$

where v_s is called the *deposition velocity*[14] and $\overline{\chi}_{m_z}$ is the mixing ratio of the gas or aerosol at level z. In the absence of scavenging by rain or snow (called *wet deposition*), this deposition velocity is used to estimate the *dry deposition* of materials with a negligible fall velocity onto the ground and vegetation surfaces. The value of v_s also depends on the chemical species involved. For SO_2, the deposition velocity is estimated to be on the order of 1 cm s^{-1}, whereas sulfates of size 0.1–1 μm are reported to have values of around 0.01–1 cm s^{-1} (Eliassen 1980). Everett *et al.* (1979) found a value of v_s = 1.4 cm s^{-1} for particulate sulfur, whereas Wesely *et al.* (1978) reports values of v_s for ozone during the daytime ranging from 0.2 to 0.8 cm s^{-1} with its peak in midmorning. Lenschow *et al.* (1981) gave a value of v_s of about 0.5 cm s^{-1} for ozone over a portion of eastern Colorado during the day. These values of v_s are for specific measurement heights (since $\overline{\chi}_{m_z}$ is a function of z).

Sheih *et al.* (1979) report on a formulation for the deposition velocity of SO_2 over land given by

$$v_{SO_2} = ku_*\left[\ln(z/z_0) + 2.6 + ku_* r_{SO_2} - \psi_H\right]^{-1}, \tag{7-43}$$

where r_{SO_2} represents the surface resistance to SO_2 uptake. For a vegetative surface, r_{SO_2} is the integrated effect of the stomatal resistance of the plants (called the *effective bulk canopy stomatal resistance*). Over water, Sheih *et al.* (1979) suggest the formulation

$$v_{SO_2} = ku_*\left[\ln(ku_* z/v_s) - \psi_H\right]^{-1}, \tag{7-44}$$

where v_s is the molecular kinematic diffusivity of SO_2 in air ($v_s \simeq 0.2$ cm^2 s$^{-1}\pm$ 50%)[15] with $r_{SO_2} = 0$, since SO_2 is highly soluble in water. Values of r_{SO_2} as a function of stability class are given in Sheih et al. (1979). The deposition velocity of sulfate aerosols over land and water is given in Sheih *et al.* (1979) as

$$v_{SO_4} = ku_*\left[\ln(z/z_0) + kr_{SO_4}u_* - \psi_H\right]^{-1}, \tag{7-45}$$

where r_{SO_4}, the surface resistance to particle deposition, is assumed to be 1 s cm^{-1}.

Additional discussions of deposition are given by Wesely and Hicks (1977), Galloway *et al.* (1980), Brook *et al.* (1999), Jackson and Lyford (1999), and Ma and Daggupaty (2000). Slinn (1982) discusses particle dry deposition to vegetation.

7.3.3 Transition Layer

The transition layer extends from h_s to z_i, which ranges from 100 m or so to several kilometers or more. Above the surface layer, the mean wind changes direction with height and approaches the *free-stream velocity* at the height z_i as the subgrid-scale fluxes $\overline{u''w''}$ and $\overline{u''v''}$ decrease in magnitude. The definition of z_i, the top of the boundary layer, is *the lowest level in the atmosphere at which the ground surface no longer influences the dependent variables through the turbulent transfer of mass.*[16] Tennekes (1974) gives a useful qualitative discussion of the atmospheric boundary layer, and Krishnamurti *et al.* (1983) discuss different types of boundary layers resulting from different sets of balance of forces: (a) a balance among Coriolis, pressure gradient, and frictional forces (an *Ekman* boundary layer); (b) a balance between the pressure gradient and frictional forces and the advective accelerations (an *advective boundary layer*); and (c) a balance between the pressure gradient and frictional forces (a *Stokes boundary layer*). When thunderstorms occur, the boundary layer can extend into

the stratosphere. However, for most applications in mesoscale models, the planetary boundary layer is between a few hundred meters and several kilometers or so above the ground.

When the bottom surface is heated, the planetary boundary layer tends to be well mixed, particularly in potential temperature. Specific humidity is somewhat less well mixed because the entrainment of dry air into a growing boundary layer permits a gradient in $\bar{q}_3$ to exist between the top of the planetary boundary layer and the (usually) more moist surface (Mahrt 1976). Because of horizontal pressure gradients, winds are the least well mixed. When the surface is cool, relative to the overlying air, vertical gradients in all of the dependent variables exist within the planetary boundary layer.

The depth of the planetary boundary layer, z_i, is usually associated with an inversion. As discussed by Oke (1978), there are three types of inversions:

- *inversions caused by cooling*: radiational cooling at night, or above stratiform clouds and smog layers, and evaporative cooling over moist ground
- *inversions caused by warming*: synoptic subsidence and cumulus-induced subsidence
- *inversions caused by advection*: frontal inversions; warm air over cold land, water, or snow; and vertical differences in the horizontal advection of temperature.

Busch *et al.* (1982) discussed the formation of inversions over huge areas in the polar region caused by several of these mechanisms. Diurnal variations in the height of the inversion and stability within the boundary layer can contribute to a large wind maximum just above z_i, as discussed by Blackadar (1957), Hoxit (1975), Zeman (1979), McNider and Pielke (1981), Arritt (1985), Arritt and Pielke (1986), and others. Large wind shears can also develop at that level, caused by increased surface-layer thermodynamic stability over land during a hurricane landfall (Powell 1982). Internal gravity waves can occur on such inversions (see Section 5.2.1.2), and can influence boundary-layer structure below that level (see, e.g., Finnegan and Finnegan 1981). Horizontal roll vortices are often observed within inversion-capped boundary layers that are heated from below.[17]

In the absence of an inversion, when the air is neutrally stratified, Blackadar and Tennekes (1968) suggested that z_i is proportional to u_*/f. In contrast, Deardorff (1972) and Mahrt (1972), as reported by Moss (1978), suggested that the lifting condensation level is the appropriate height.

Formulations for the depth of the nocturnal boundary layer have been suggested by Yu (1978), Nieuwstadt and Driedonks (1979), Yamada (1979a), Zeman (1979), Mahrt (1981a), Nieuwstadt and Tennekes (1981), Wetzel (1982), Stull (1983), and others. Tomasi (1983) has evaluated the use of several of these

schemes to predict the height of the nocturnal inversion in Italy's Po Valley during stagnate, clear synoptic conditions. In Yamada's formulation, nocturnal longwave radiational cooling is included. Gopalakrishnan (1996) concluded that with light winds on clear nights, radiational cooling dominates the creation of the nocturnal boundary-layer depth. Sharan and Gopalakrishnan (1997) evaluate several parameterizations of turbulence in strongly and weakly stable boundary layers.

Mahrt (1981b) has studied the transition of a daytime mixed layer to a nocturnal boundary layer. He found that the ageostrophic wind increases during the transition because the surface shearing stress decreases more slowly than does the downward transport of momentum associated with the decreased depth of turbulence; therefore, the winds turn more toward lower pressure. André and Mahrt (1982) conclude that for the observational datasets in clear sky conditions which they investigated, the lower part of the nocturnal inversion is turbulent, although strongly stratified, while the upper portion, despite its weaker stratification, is created almost completely by longwave radiative flux divergence. Arya (1981) provides a brief summary of proposed diagnostic and prognostic relations for parameterizing the height of the nocturnal boundary layer. Mahrt (1983) gives a brief survey of studies on stably stratified boundary layers. Dayan and Rodnizki (1999) provide a summary of the behavior of a boundary layer over Israel for a 3-year period.

Variations of the planetary boundary-layer depth caused by subgrid-scale fluxes need not be parameterized when a local representation to the exchange coefficients are used, but will appear through changes in the vertical profile of the dependent variables. However, when a well-defined inversion is present, it is useful to include an equation that represents its change over time.

When the surface layer is superadiabatic (i.e., $\partial\bar{\theta}/\partial z<0$), a simplified boundary-layer formulation, called a *jump model*, has been proposed (e.g., Ball 1960; Lilly 1968; Tennekes 1973; Deardorff 1974a; Driedonks 1982a). Illustrated in Figure 7-8, this model has a potential temperature discontinuity at z_i of a magnitude of $\Delta\theta_i$. Below z_i, the turbulent flux of heat, $\overline{w''\theta''}$ is assumed to decrease linearly with height and to become negative in the upper boundary layer, with its minimum value of $\overline{w''_{z_i}\theta''_{z_i}}$ at the inversion. Above z_i, the lapse rate, defined as $\partial\bar{\theta}^+/\partial z$, is stably stratified. Such a boundary layer is called a *mixed layer*, because the dependent variables, particularly $\bar{\theta}$, tend to be uniformly distributed with height.

In this representation, following the discussions of Lilly (1968) and Tennekes (1973), the growth of z_i is given by

$$(dz_i/dt)-\bar{w}_{z_i}=-\overline{w''_{z_i}\theta''_{z_i}}/\Delta\bar{\theta}_i, \tag{7-46}$$

where $\bar{w}_{z_i}$ represents mesoscale or synoptic vertical motion, or both, at z_i. When $\bar{w}_i=0$, the change in height of z_i with time depends on the rate of entrainment

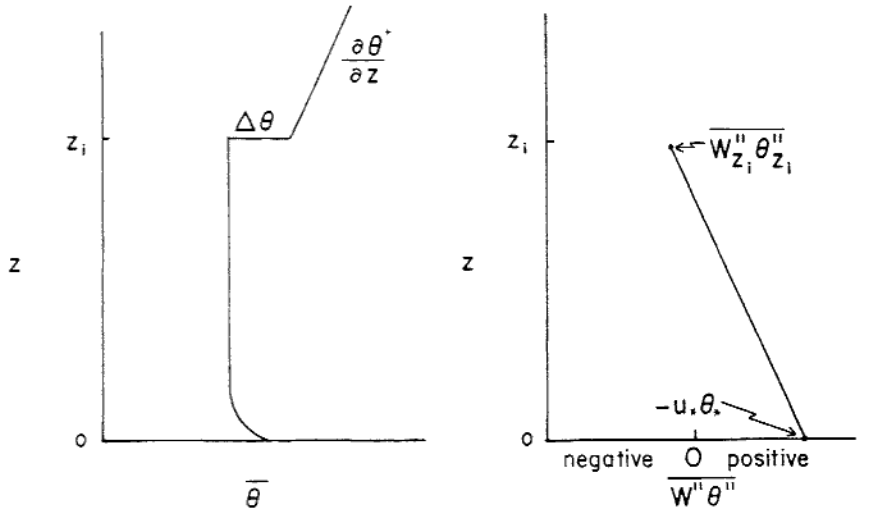

Fig. 7-8. The potential temperature and heat flux profiles assumed in the "jump" model.

of mass into the boundary layer.[18] The prognostic expression for $\Delta\bar{\theta}_i$ is

$$\frac{d\Delta\bar{\theta}_i}{dt} = \left(\frac{dz_i}{dt} - \bar{w}_{z_i}\right)\frac{\partial\bar{\theta}^+}{\partial z} + \frac{\overline{w''_{z_i}\theta''_{z_i}} - \overline{w''_s\theta''_s}}{z_i}, \tag{7-47}$$

where $\overline{w''_s\theta''_s}$ is the surface heat flux equal to $-u_*\theta_*$ from Eq. (7-29). The first term on the right side of Eq. (7-47) represents the tendency to increase $\Delta\bar{\theta}_i$ as the boundary layer rises, whereas the second term tends to decrease $\Delta\bar{\theta}_i$ as the layer warms from the surface. To specify the heat flux at z_i in terms of the surface heat flux, the assumption is made that

$$\overline{w''_{z_i}\theta''_{z_i}} = -\alpha\overline{w''_s\theta''_s} = +\alpha u_*\theta_*, \tag{7-48}$$

where $\alpha = 0.2$ is usually used (e.g., Yamada and Berman 1979; Driedonks 1982b). Stull (1976) summarized published values of α obtained from observations, while Betts *et al.* (1992), and Hägeli *et al.* (2000) reported on values of α that are quite different than 0.2. Sun (1993a) concluded that representing entrainment in such a simple form does not work very well when clouds are present such that evaporation and radiative cooling can produce negative buoyancy at the inversion height. If $d\Delta\theta_i/dt$ is assumed to be small relative to the other two terms in Eq. (7-47), then Eq. (7-47) can be written as

$$\frac{dz_i}{dt} = \bar{w}_{z_i} = -\frac{1.2u_*\theta_*}{z_i\partial\bar{\theta}^+/\partial z} \tag{7-49}$$

Deardorff (1974a) has improved on the formulation given by Eq. (7-49) using his three-dimensional numerical planetary boundary-layer simulation of Day 33 of the Wangara Experiment (Clarke *et al.* 1971). Deardorff's (1974a) parameterization has subsequently been adopted by Pielke and Mahrer (1975) and others and shown to be very realistic when the variation of z_i with time is strongly influenced by surface heating. This prognostic representation for the planetary boundary-layer height can be written as

$$\frac{\partial z_i}{\partial t} = -\bar{u}_{z_i}\frac{\partial z_i}{\partial x} - \bar{v}_{z_i}\frac{\partial z_i}{\partial y} + \bar{w}_{z_i} + \left[1.8(w_*^3 + 1.1u_*^3 - 3.3u_*^2 f z_i)\right] \Big/ \left(g\frac{z_i^2}{\bar{\theta}_{h_s}}\frac{\partial \bar{\theta}^+}{\partial z} + 9w_*^2 + 7.2u_*^2\right), \tag{7-50}$$

where

$$w_* = \begin{cases} \left(-\frac{g}{\bar{\theta}_{h_s}} u_* \theta_* z_i\right)^{1/3}, & \theta_* \le 0 \\ 0, & \theta_* > 0 \end{cases}$$

and $\bar{\theta}_{h_s}$ is the potential temperature at the top of the surface layer. The scaling velocity, w_*, has been called the convective velocity scale, or the Deardorff velocity (Stull 2000). As in Eq. (7-49), in Eq. (7-50) the growth of z_i is directly proportional to the surface heat flux and mesoscale vertical velocity and inversely proportional to the overlying stability.

Equation (7-50) can also be used to estimate $\bar{w}_{z_i}$ if it is assumed the boundary-layer height is unchanging over time and horizontally homogeneous, $\theta_* = 0$, and the net radiational flux divergence is 0. For this case, Eq. (7-50) reduces to

$$\bar{w}_{z_i} = -\left(1.98u_*^3 - 5.94u_*^2 f z_i\right) \Big/ \left(g\frac{z_i^2}{\bar{\theta}_{h_s}}\frac{\partial \bar{\theta}^+}{\partial z} + 7.2u_*^2\right),$$

where z_i is obtained from a radiosonde or other observational platform. For example, with typical values of $u_* = 50\ \mathrm{cm\,s^{-1}}$, $f = 10^{-4}\mathrm{s^{-1}}$, $\theta_{h_s} = 300$ K, $\partial\bar{\theta}^+/\partial z = 1°/100$ m, and $z_i = 1$ km, we have $\bar{w}_{z_i} = 0.03\ \mathrm{cm\,s^{-1}}$.

When $\theta_* = 0$, $\bar{w}_{z_i} = 0$, $\partial\bar{\theta}^+/\partial z = 0$, and $dz_i/dt = 0$, Eq. (7-50) reduces to $z_i = 0.33u_*/f$, which is the expected depth of the planetary boundary layer in a steady-state, horizontally homogeneous, neutrally stratified boundary layer. Obviously, this latter representation for a neutral boundary layer must be modified in the tropics, where f approaches 0.

The height of the surface layer, h_s, can be estimated from z_i as

$$h_s = 0.04 z_i. \tag{7-51}$$

For example, with $z_i = 1$ km, $h = 40$ m. This formulation was based on the results of Blackadar (1972, personal communication) and Blackadar and Tennekes (1968), who found the best agreement between their predictions and

observations in a neutrally stratified boundary layer when Eq. (7-51) was adopted.

When clouds are present at the top of the mixed layer, the effect of cumulus-induced subsidence must be included in the $\bar{w}_{z_i}$ term in Eq. (7-50). Brost *et al.* (1982a, b) discussed the mean and turbulent budgets in a marine stratocumulus-topped mixed layer off the California coast, and Augstein and Wendel (1980) presented a one-dimensional tradewind boundary-layer model with nonprecipitating cumulus clouds. Chen and Cotton (1983b) discussed a one-dimensional simulation of a stratocumulus-capped mixed layer in which the relative importance of turbulence, radiation, and subgrid-scale cloud condensation are contrasted.

In Augstein and Wendel's study, the authors concluded that radiation was as important in boundary-layer development as large-scale subsidence and the horizontal advection of heat and water vapor. According to their model calculations, solar heating reduces the effect of both condensational heating within the active cloud layer and evaporative cooling at the top of the cloud layer, as compared to that occurring at night. This response, resulting from the dependence of saturation specific humidity on temperature, results in deeper clouds at night because the cumulus convection is more vigorous in the absence of this solar heating.

7.3.3.1 Idealized Theory

An idealized representation of the winds in the transition layer can be derived from a simplified form of Eq. (4-21) given in component form by

$$\begin{aligned} 0 &= K\frac{\partial^2 \bar{u}}{\partial z^2} + f(\bar{v} - v_g) \\ 0 &= K\frac{\partial^2 \bar{v}}{\partial z^2} + f(u_g - \bar{u}), \end{aligned} \tag{7-52}$$

where only the large-scale horizontal pressure gradient term (as represented by the geostrophic wind components u_g and v_g [see, e.g., Eq. (3-28)], the Coriolis terms $f\bar{u}$ and $f\bar{v}$, and the vertical subgrid flux terms are retained. The geostrophic wind is assumed to be constant with height, whereas the subgrid-scale flux terms are approximated with a constant exchange coefficient K. The horizontal wind components $\bar{u}$ and $\bar{v}$ do not vary with time or in the x and y directions. An atmosphere represented by these two equations is in steady-state equilibrium and horizontally homogeneous.

Following Dutton (1976:449), these equations can be written using complex notation as

$$0 = \frac{\partial^2 V_H}{\partial z^2} + i\frac{f}{K}(V_G - V_H), \tag{7-53}$$

where $V_H = \bar{u} + i\bar{v}$ and $V_G = u_g + iv_g$. Substituting V_H into Eq. (7-53), it is straightforward to show that

$$V_H - V_G = a_1 \exp\left[(1+i)l_E^{-1}z\right] + a_2 \exp\left[-(1+i)l_E^{-1}z\right],$$

where $l_E = \sqrt{2K/f}$.

The boundary conditions needed to solve this equation are

$$V_H = 0 \quad \text{at} \quad z = 0 \qquad \text{and} \qquad \lim_{z\to\infty} V_H = V_G.$$

Therefore, a_1 must equal 0 and $a_2 = -V_G$, so that

$$\begin{aligned} V_H - V_G &= -V_G \exp\left[-1(1+i)l_E^{-1}z\right] \\ &= -V_G e^{-z/l_E}\left[\cos(z/l_E) - i\sin(z/l_E)\right], \end{aligned} \tag{7-54}$$

where $z = \pi l_E \simeq z_i$ is a representative depth for the boundary layer (i.e., the first level above the ground where $V_H = V_G$), assuming that Eq. (7-52) is applicable. The solution to Eq. (7-54) for particular values of f and K is plotted in Figure 7-9. In the northern hemisphere, where $f > 0$, the winds near the surface, according to Eq. (7-54), are to the left of the geostrophic wind (i.e., toward low pressure). The wind *veers* (i.e., turns clockwise) with height and slightly overshoots the geostrophic value. This spiral wind profile, called the *Ekman profile*, is useful in the initialization of mesoscale models, as illustrated by Eq. (11-13) in Chapter 11. The transition layer is also called the *Ekman layer*, because this is that section of the planetary boundary layer in which the average wind direction changes with height. Kahl and Samson (1988) and Moran and Pielke (1996a, b) have shown how such wind shear influences the transport and dispersion of pollution.

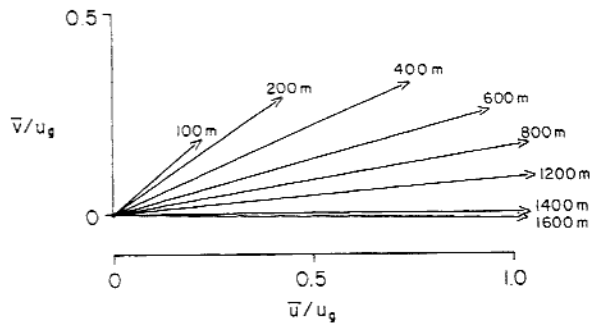

Fig. 7-9. A plot of the Ekman wind using Eq. (7-54), with $f = 10^{-4}$ and $K = 10\ \text{m}^2\,\text{s}^{-1}$; $l_E = 450$ m and $z_i \simeq 1400$ m. Without loss of generality, the components of Eq. (7-54) can be written as $\bar{u} = u_g(1 - e^{-z/l_E}\cos z/l_E)$ and $\bar{v} = u_g e^{-z/l_E}\sin z/l_E$ by setting $v_g = 0$, which is how they are displayed in this figure. Rotating the figure through the angle given by the arctangent of v_g/u_g gives the solution of Eq. (7-54) for any direction of the geostrophic wind.

7.3.3.2 Parameterization of the Transition Layer

The parameterization of the subgrid-scale correlation terms in the planetary boundary layer can be grouped into four categories:

- drag coefficient representations
- local exchange coefficients
- exchange coefficients derived from profile functions
- explicit equations for the subgrid-scale fluxes.

The first three classes above are often called *first-order closure representations*, because the subgrid-scale correlations are specified as functions of one or more of the grid-volume–averaged dependent variables $(\bar{u}_i, \bar{\theta}, \bar{q}_n, \overline{\chi}_m)$. The fourth category is called *second-order closure*, because prognostic equations are developed for the fluxes,[19] which include triple-correlation terms involving subgrid-scale variables [e.g., $\overline{u_j'' \partial e/\partial x_j}$ in Eq. (7-5)] that must be represented in terms of the double-correlation terms or the averaged dependent variables or both. The procedure to obtain the prognostic equations for the subgrid-scale fluxes $(\overline{u_j'' u_i''}, \overline{u_j'' \theta''}, \overline{u_j'' q_n''}$, and $\overline{u_j'' \chi_m''})$ was presented in Section 7.1.

Lewellen (1981), Zeman (1981), Mellor and Yamada (1982), and Wyngaard (1982) provide derivations and discussion of second-order equations, and Mellor and Yamada (1974) discuss the different levels of complexity using various simplifications of these explicit representations of the subgrid-scale fluxes. Yamada (1979b) performed a planetary boundary-layer analysis using one level of the Mellor–Yamada formulation. Libersky (1980, Table 2) provides an effective summary of approximations to the terms in second-order closure models, and Burk (1981) and Lewellen *et al.* (1983) provide other examples of simulations using second-order models. As illustrated in Section 7.3.3.4; accurate parameterizations of the planetary boundary layer in mesoscale models can be obtained without using second-order closure, despite arguments to the contrary suggested by such investigators as Zeman (1981).

The drag coefficient form (also called the *bulk aerodynamic* formulation) is given by, for example,

$$\overline{w'' u''} = -C_D \overline{V}^2 \cos\mu, \quad \overline{w'' v''} = -C_D \overline{V}^2 \sin\mu, \quad \text{and}$$
$$\overline{w'' \theta''} = C_D' \overline{V} (\bar{\theta}(z_0) - \bar{\theta}), \tag{7-55}$$

where $\overline{V}$ and $\bar{\theta}$ are evaluated at some height within the surface layer (often 10 m) with μ equal to the arctan $(\overline{V}/\bar{u})$. The parameters C_D and C_D' are called *drag coefficients*. Above this level, a local exchange coefficient form is sometimes used if there is vertical resolution within the boundary layer. Rosenthal (1970), Lavoie (1972), and others have obtained realistic simulations using this form. Rosenthal used a value of $C_D = 3 \times 10^{-3}$ for velocity and $C_D' = 0$ for heat and moisture. Lavoie used $C_D = 7 \times 10^{-3}$ over land and $C_D = 1.5 \times 10^{-3}$ over water

for velocity, and used $C_D' = 1.5 \times 10^{-3}$ for heat if the surface layer was defined to be superadiabatic and $C_D' = 0$ otherwise. Fujitani (1981) presents observational estimates of the drag coefficient as measured over the East China Sea with mean values of $C_D = 1.3 \times 10^{-3}$ and $C_D' = 1.2 \times 10^{-3}$, although both values were lower for stable surface conditions. In that study, C_D had a larger value of about 2.1×10^{-3}, with high variability, for light winds ($\overline{V}$ less than 4 m s^{-1}).

Because using Eq. (7-16), $u_*^2 = C_D \overline{V}^2$ from Eq. (7-55), and by Eq. (7-29), $u_* \theta_* = C_D' \overline{V}(\bar{\theta} - \bar{\theta}(z_0))$ from Eq. (7-55), substituting for $\overline{V}$ from Eq. (7-27) and $\bar{\theta} - \bar{\theta}(z_0)$ from Eq. (7-31), and rearranging yields the expressions for C_D and C_D' given by[20]

$$C_D = k^2 \Big/ \left[\ln \frac{z}{z_0} - \psi_M \left(\frac{z}{L} \right) \right]^2$$
$$C_D' = \beta k^2 \Big/ \left[\ln \frac{z}{z_0} - \psi_M \left(\frac{z}{L} \right) \right] \left[\ln \frac{z}{z_0} - \psi_H \left(\frac{z}{L} \right) \right]. \tag{7-56}$$

Thus, except for special cases such as when the winds are strong [so that $\psi_M(z/L) = \psi_H(z/L) \simeq 0$] and the aerodynamic roughness of the surface is unchanging, it is inappropriate to treat the drag coefficient as a constant. Using drag coefficients, fluxes in the boundary layer can be represented by requiring $C_D = C_D' = 0$ at z_i with a specified functional form between the surface and z_i.

The use of exchange coefficients is of the form given by Eq. (7-7), for example, where K_θ and K_m are exchange coefficients. If these coefficients are defined only in terms of local gradients, then they are called *local exchange coefficients*, but if they are derived from a vertical interpolation formula that is independent of local gradients, then they are called *profile coefficients*. Blackadar (1979) suggested one form of local exchange coefficient when the layer being simulated is stably stratified air ($\partial \bar{\theta} / \partial z > 0$), which is expressed as[21]

$$K_m = K_\theta = \begin{cases} 1.1(\mathrm{Ri_C} - \mathrm{Ri}) l^2 |\partial \vec{V} / \partial z| / \mathrm{Ri_C}, & \mathrm{Ri} \le \mathrm{Ri_C} \\ 0, & \mathrm{Ri} > \mathrm{Ri_C}, \end{cases} \tag{7-57}$$

where l is a mixing length and $\vec{V} = \bar{u}\vec{i} + \bar{v}\vec{j}$. In the form used by McNider (1981) and McNider and Pielke (1981), l is given as

$$l = \begin{cases} kz, & z < 200 \text{ m} \\ 70 \text{ m}, & z \ge 200 \text{ m}. \end{cases}$$

The parameter $\mathrm{Ri_C}$ is the critical Richardson number, described following Eq. (7-8), which should equal 0.25 in the limit as the vertical grid spacing approaches 0. The finite difference value of $\mathrm{Ri_C}$ increases as the vertical grid increment increases, as discussed by, for example, Shir and Bornstein (1977).

Another example of a local exchange coefficient representation is that of Orlanski *et al.* (1974), where K_m and K_θ vary from a background value of these coefficients only when $\partial\bar{\theta}/\partial z < 0$. Klemp and Lilly (1978) use a form of mixing equivalent to a local exchange coefficient, which requires that the Richardson number in their model always equal or exceed the critical Richardson number, 0.25. A local exchange coefficient is appropriate when the vertical grid resolution is high (so that the gradients can be accurately approximated), when horizontal advection of turbulence is small, and when the characteristic length scales of the subgrid-scale mixing are approximately the same size or less than twice the vertical grid spacing.[22]

With such a representation, fluxes are always *downgradient*, since $K_m = K_\theta \geq 0$ (i.e., toward smaller values of $\bar{u}$, $\bar{v}$, $\bar{\theta}$, $\bar{q}_n$, and $\overline{\chi_m}$). As shown by Deardorff (1966), however, *countergradient* fluxes are known to occur when the surface layer is superadiabatic (i.e., $z/L < 0$). Deardorff suggested that the vertical gradient of potential temperature used in the representation $\overline{w''\theta''} = -K_\theta \partial\bar{\theta}/\partial z$ be modified to $\overline{w''\theta''} = -K_\theta \partial\bar{\theta}_C/\partial z$ with

$$\frac{\partial\bar{\theta}_C}{\partial z} = \frac{\partial\bar{\theta}}{\partial z} - \gamma_C, \tag{7-58}$$

where $\gamma_C = 0.65 \times 10^{-3}$ K m^{-1} to permit fluxes of heat upgradient. Tijm et al. (1999a), based on Holtslag and Boville (1993) and Holtslag *et al.* (1995), expressed the countergradient flux effect for $z/L \ll 0$ in the following form:

$$\overline{w''\theta''} = -K_\theta \left(\frac{\partial\bar{\theta}}{\partial z} - \gamma_C \right), \tag{7-59}$$

where

$$K_\theta = 1.4 k w_* z \left(1 - \frac{z}{z_i} \right)^2, \tag{7-60}$$

with w_* defined as

$$w_* = \left(\frac{-g}{\theta_{h_v}} u_* \theta_* z_i \right)^{1/3}. \tag{7-61}$$

The countergradient term in Eq. (7-59), expressed using the variables defined in this chapter, is

$$\gamma_C = -10 \frac{u_* \theta_*}{w_* z_*}. \tag{7-62}$$

K_θ is an example of an exchange coefficient derived from a profile function.

7.3.3.3 Parameterization Complexity

It is useful to dissect a parameterization algorithm to determine the number of dependent variables and adjustable and universal parameters that are introduced. This dissection can be illustrated through the following simple example. Holtslag and Boville (1993) and Tijm et al. (1999a) propose the following form for K_θ above the boundary layer:

$$K_\theta = l_\theta^2 S F_\theta(\mathrm{Ri}), \tag{7-63}$$

where

$$\frac{1}{l_\theta} = \frac{1}{kz} + \frac{1}{\lambda_\theta}, \tag{7-64}$$

$$S = \left| \frac{\partial \vec{V}}{\partial z} \right|, \tag{7-65}$$

and

$$F_\theta(\mathrm{Ri}) = \begin{cases} (1 - 18\ \mathrm{Ri})^{1/2}, & \mathrm{Ri} \le 0 \\ 1/(1 + 10\ \mathrm{Ri} + 80\ \mathrm{Ri}^2), & \mathrm{Ri} > 0, \end{cases} \tag{7-66}$$

with

$$\lambda_\theta = \begin{cases} 300\ \mathrm{m}, & z \le 1\,\mathrm{km} \\ 30\ \mathrm{m} + 270 \exp(1 - (z/1000\ \mathrm{m})). \end{cases} \tag{7-67}$$

This formulation for K_θ includes the following dependent variables, parameters, and prescribed constants:

- In Eq. (7-63), the dependent variables l_θ, S, and F_θ define K_θ.
- In Eq. (7-64), l_θ is defined with the independent variable z, the dependent variable λ_θ, and the parameter k.
- In Eq. (7-65), S is defined by the vertical gradient of $\vec{V}$.
- In Eq. (7-66), F_θ (Ri) is defined by the dependent variable Ri [which is defined by Eq. (7-8)] and the constants 18, 10, and 80 and the exponent 1/2.
- In Eq. (7-67), λ_θ is defined by the independent variable z and the constants 300, 30, 270, and 1000.

Therefore, to represent the term K_θ, in addition to the fundamental variables $\bar{u}_i$ and $\bar{\theta}$, one parameter (k) and eight constants (18, 10, 80, 1/2, 300, 30, 270, 1000) must be provided.

A sensitivity analysis can be applied to show how K_θ responds to slight changes in the dependent variables and constants. For example, in Eq. (7-67), if 100 m were used instead of 300 m when λ_θ dominates in Eq. (7-64), then K_θ would be 1/9 as large, since K_θ is proportional to l_θ^2. Clearly, the form of

Eq. (7-67) will exert a major effect on the parameterized turbulent mixing in a model.

Niyogi *et al.* (1999) discuss such a sensitivity analysis (in their case for surface fluxes) in terms of the question "What scenarios make a particular parameter significant?" They also appropriately conclude that parameter uncertainty is not only related to its deviation, but is also dependent on the values of the other parameters used in a parameterization.

7.3.3.4 Parameterization Comparisons

Various forms of the explicit representation of the subgrid-scale fluxes [e.g., $(\partial/\partial t)\overline{u_j'' u_i''}$, $(\partial/\partial t)u_j'' \theta''$] have been used by Donaldson (1973), Deardorff (1974a, b), Lumley and Khajeh-Nouri (1974), Wyngaard and Coté (1974), Burk (1977), André *et al.* (1978), Brost and Wyngaard (1978), Gambo (1978), Lee and Kao (1979), Abdella and McFarlane (1997, 1999), Mironov et al. (1999), and others. As mentioned earlier in this chapter, Mellor and Yamada (1974) categorized the level of complexity of those second-order representations. Although theoretically more satisfying, this more expensive approach, with its greater degrees of freedom, has not improved simulations of the evolution for the resolvable dependent variables in the planetary boundary layer over those obtained using the best first-order representations.

For example, Days 33 and 34 of the Wangara Experiment (Clarke *et al.* 1971) has been used extensively to examine the accuracy of various parameterizations of the planetary boundary layer. Deardorff (1974a), Wyngaard and Coté (1974), Pielke and Mahrer (1975), Yamada and Mellor (1975), Dobosy (1979), Sun and Ogura (1980), Blondin and Therry (1981), Mailhot and Benoit (1982), Chen and Cotton (1983a), Therry and Lacarrere (1983), Sun (1993a), and Finkele (1998), among others, have attempted to simulate boundary layer structure for all or a portion of these days. Figure 7-10(a), reproduced from the sophisticated higher-order model of André *et al.* (1978), illustrates the evolution of the averaged vertical potential temperature in the boundary layer using a model that has an explicit representation of the subgrid-scale fluxes. Figure 7-10(b) shows the results for the same period using first-order closure, as described in McNider and Pielke (1981), to represent the vertical exchange coefficient.

Both results closely correspond to the observed profile [Figure 7-10(c)]. The profiles of the other dependent variables produced by the two models also closely agree. Yu's (1977) results support part of this conclusion in that he found that using the McNider and Pielke (1981) parameterization produced accurate simulations of the growth of the mixed layer when compared to a range of other schemes, including a simplified second-order representation.

Sharan and Gopalakrishnan (1997) provide another comparison study of the accuracy of several turbulent closure schemes in terms of their ability

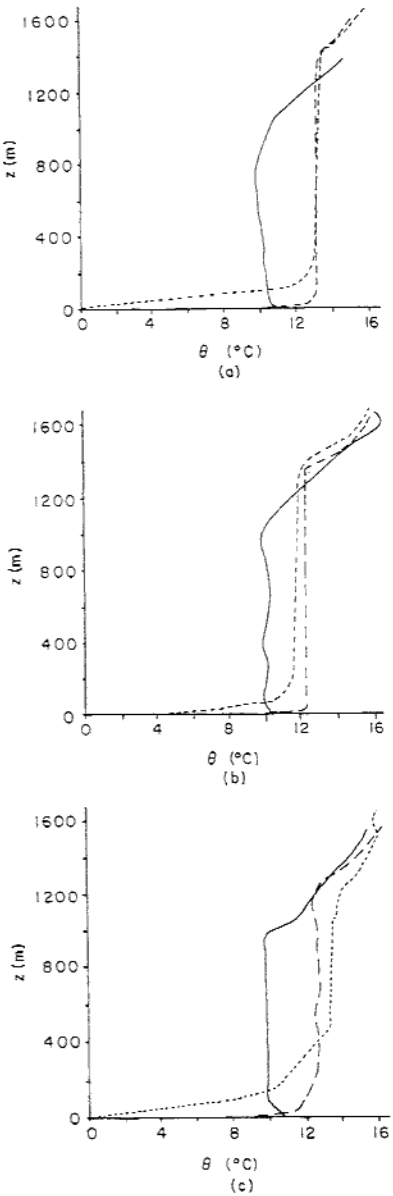

Fig. 7-10. Comparison of predictions using (a) higher-order closure (André *et al.* 1978) for Day 33–34 of the Wangara Experiment, (b) first-order closure (McNider and Pielke 1981), and (c) observational data presented by André *et al.* (1978). The solid and dashed lines correspond to 1200 LST and 1800 LST on Day 33; the dotted line corresponds to 0300 LST on Day 34.

to represent the stable boundary layer. Another modeling study of several boundary-layer parameterizations is discussed in Alapaty and Mathur (1998).

Zeman (1979) claims that his economical one-layer model compares favorably against second-order closure models in simulating the evolution of a nocturnal boundary layer. Klöppel *et al.* (1978) showed that the development and decay of ground-based inversions can be satisfactorily simulated by simple models. Chang (1979) produced accurate results using a Richardson number adjustment scheme for heat and momentum exchanges and concluded that this method provides an economical and realistic alternative to higher-order closure schemes.

Finally, investigators such as Mailhot and Benoit (1982) have suggested that an exchange coefficient must depend on the past history of the flow, so they use a coefficient that is dependent on the second-order property $\frac{1}{2}\bar{u}_i''^2$ and a length scale. However, the first-order exchange coefficients (which are dependent only on resolvable quantities, such as, $\bar{u}_i$ and $\bar{\theta}$) also depend on the history of the flow, since the resolvable variables themselves were determined in part from the response to turbulent mixing at previous times. Therefore, contrary to the conclusion of Mailhot and Benoit, unless significant turbulent (i.e., subgrid-scale) energy created at one grid point is *advected or diffused* to another grid cell, it appears unnecessary to include any prognostic equations for the second-order terms to parameterize the influence of subgrid-scale mixing on the grid-volume–averaged flow in mesoscale models.

Second-order closure boundary-layer models, of course, remain valuable tools to use in developing the most accurate first-order closure schemes and in developing effective parameterizations of the diffusion of pollutants, as described in Zannetti (1990), Uliasz *et al.* (1996), and Sharan *et al.* (1999). Of even more value, however, may be the use of large-eddy simulation (LES) models (e.g., such as reported in Bader and McKee 1983) to determine small-scale responses over nonhomogeneous terrain to specific sets of mesoscale forcing. Deardorff (1974a) has used this approach very effectively to develop parameterizations of mixed layer height for use in mesoscale models. A model is an LES when the model-resolved fluxes are much larger than the subgrid-scale fluxes (e.g., $|\overline{w''\theta''}| \ll |\bar{w}\bar{\theta}|$).

Examples of studies of using LES modeling to improve our understanding of homogeneous and nonhomogeneous landscapes on the convective boundary layer include Avissar and Schmidt (1998), Avissar *et al.* (1998), Stevens *et al.* (1998, 1999), Gopalakrishnan and Avissar (2000), and Gopalakrishnan *et al.* (2000). Mason and Brown (1999) used high-resolution LES modeling to conclude that length scales of turbulence should be buoyancy dependent, and to increase with unstable buoyant transfer.

7.4 Heterogenous Boundary Layers

When the surface is unevenly heated, or of different aerodynamic roughness, even though it is flat, the resultant surface and boundary-layer fluxes will be different (see, e.g., Vickers and Mahrt 1999). As air blows across this landscape, air near the surface will be directly responding to the turbulent fluxes which result from that surface, while air higher up will be still responding to the fluxes that resulted from the passage of the air over the original surface. The interface between these two sources of turbulent fluxes is called the *internal boundary layer*. Figures 7-11 and 7-12 illustrate schematically the behavior of the internal boundary layer for several different spatial distributions of surface heterogeneity. Examples of recent papers that discuss the internal boundary layer include Batchvarova *et al.* (1999) and Jegede and Foken (1999).

An internal boundary layer resulting from spatially varying surface turbulent sensible heat fluxes is called a *thermal internal boundary layer*. Turbulence that remains above the internal boundary layer will leave an altered vertical and horizontal structure of the temperature, winds, and other variables once it decays. This remnant of the turbulence is called *fossil turbulence* (Gibson 1999). Nieuwstadt and Brost (1986) estimate that it can take up to an hour or so for surface-forced convective eddies to decay once surface heating is removed. Mahrt (2000) concludes that internal boundary layers have more a diffuse vertical structure than textbook examples—a result, perhaps, of the heterogenous character of real world landscapes.

As discussed by Kerman (1982) and others, the growth of such a boundary layer can substantially influence the occurrence and location of fumigation in coastal regions. It can also influence the propagation of electromagnetic radiation (e.g., Gossard 1978) and the diffusion of pollutants (e.g., Gryning and

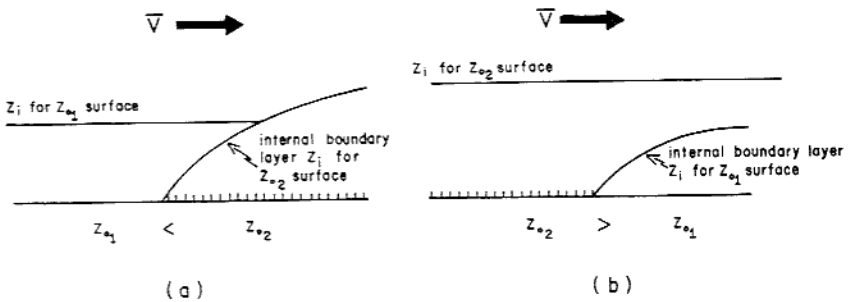

Fig. 7-11. Schematic illustration of the growth of an internal boundary layer with a neutrally stratified surface layer as airflow advects (a) from a smooth (small z_0) to a rough surface (large z_0); and (b) from a rough (large z_0) to a smoother (small z_0) surface. Note that for (a), eventually only one planetary boundary layer remains, whereas for (b), two levels of z_i remain, with separate and distinct regions of turbulence that last until the turbulent kinetic energy in the upper layer decays by dissipation.

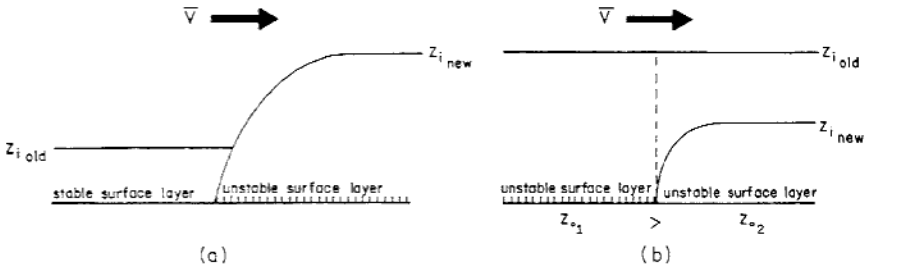

Fig. 7-12. Schematic illustration of the growth of an internal boundary layer as air advects (a) from a stably stratified surface to a region with an unstably stratified surface layer, and (b) from one unstably stratified region to another in which the equilibrium height of z_i over the new surface is lower.

Larsen 1981). Olsson and Harrington (2000) simulated the growth of an internal cloudy boundary layer as air flowed off of sea ice to over a relatively warm ocean surface. Physick *et al.* (1989) investigated how well a mesoscale model could simulate an internal boundary layer.

Onishi (1968), Peterson (1969), and others have numerically simulated changes in surface-layer structure caused by inhomogeneous terrain using two-dimensional, steady-state models. Peterson showed that in neutrally stratified air, the internal boundary layer grows about 1 unit upward for its first 10 units downstream of a change in surface characteristics. He further claims that the horizontal fetch must be 100 times its height for the new boundary layer to be equilibrium.

In an unstably stratified lower boundary layer, the growth of the internal boundary layer should be more rapid, as shown by Venkatram (1977), Højstrup (1981), Gamo *et al.* (1983), and others, since the rate of growth is coupled with the surface heat fluxes [see, e.g., Eq. (7-50)]. Højstrup reported that the growth of the internal boundary layer in the direction of the mean wind n can be written as

$$\partial z_{\mathrm{IBL}}/\partial n = D\sigma_w/\overline{V},$$

where D is a constant of order 1 and σ_w is the standard deviation of the vertical velocity as a function of height after z_{IBL} has reached its equilibrium value. With a highly unstable surface layer, $\overline{V}$ is almost constant with height (except very close to the ground). Since σ_w reaches a maximum in the midlevels of the boundary layer (see, e.g., McNider 1981), z_{IBL} will have its largest increases for a given downwind distance at those levels. Higher up, as σ_w approaches 0, the growth rate diminishes. From Højstrup's results, the ratio of the rate of growth of z_{IBL} to the distance traveled downstream during its early development was about 1–7 for the most unstable case examined and approximately 1–10 for the most neutral situation. Venkatram (1977) concluded that the growth of such internal mixed layers is enhanced by an increase of roughness, z_0, an increase of the

temperature difference between the new and original surfaces, and a decrease in the prevailing wind speed, $\overline{V}$. Venkatram's results agree closely with the observational results of Raynor *et al.* (1974). However, slower growth, occurs when the surface layer is stably stratified (e.g., Mulhearn 1981). For example, Lyons (1975) reported growth of a boundary layer to only 375 m even after several days of transit over cold ocean waters.

If the development of the internal mixed layer of 1 unit upward for 10 units downstream is used as the slowest growth rate (i.e., for $\theta_* = 0$), then a 10-km horizontal distance should be sufficient to generate a 1-km–deep planetary boundary layer. (The degree and the heights to which this mixed layer is in equilibrium with its new surface needs to be investigated further, however.)

When $\theta_* < 0$, the growth rate would be greater, as previously discussed. Hsu's (1973) observations support the rapid growth of a heated boundary layer after a change in surface characteristic from relatively cool ocean to land during the daytime over Florida. Using two towers, one of 10-m elevation over a beach and one of 100-m elevation 10 km inland, he found that the observations agreed closely with surface-layer theory developed for horizontally homogeneous steady conditions. Similarly, Kerman *et al.* (1982) found a rapid adjustment toward equilibrium ($\sim$10 km inland) as cold air over Lake Erie advected onshore over warm land. Additional detailed observations, such as those performed by Vugts (1980) and Gamo *et al.* (1982), provide further insight into the growth of the heated internal boundary layer.

These studies indicate that the larger the horizontal grid increment, the more appropriate it is to represent the boundary-layer structure as being in local equilibrium after a change of surface temperature and roughness, with the most rapid adjustment occurring when the surface layer is very unstable. Unfortunately, larger grid increments reduce the horizontal resolution so that the gains in consistency using boundary-layer theory, which is strictly valid only for horizontally homogeneous conditions, must be weighed against the need for greater spatial resolution of the forcing.

If the original surface is unstably stratified near the ground, then two layers of different turbulent characteristics can still result if the equilibrium z_i value of the downwind surface is less than that of upwind surface [e.g., caused by a smaller z_0, as illustrated in Figure 7-12(b)]. For this situation, turbulence formulations that are parameterized in terms of z_i will fail to provide proper estimates of mixing within the upper layer, although the lower region should be represented satisfactorily. In the upper region, a formulation such as that applied by McNider (1981), based on the work of Panofsky *et al.* (1960) and Blackadar (1979) and given by

$$K_m = K_\theta = (1 - 18\mathrm{R_i})^{+1/2} l^2 |\partial \vec{V}/\partial z|,$$

could be used. [Here l can be defined using formulas such as Eq. (7-64) or the definition of l following Eq. (7-57).] This relation can also be used when air

with $\partial\bar{\theta}/\partial z < 0$ advects over a region that has a stably stratified ($\theta_* > 0$) surface layer.

Studies that evaluate the effect of spatially varying heat fluxes include Hadfield *et al.* (1991, 1992), Serreze *et al.* (1992), Walko *et al.* (1992), Avissar and Schmidt (1998), Banta *et al.* (1998), Liston and Sturm (1998), Burba *et al.* (1999), Cai (1999), Hasager and Jensen (1999), Laubach and Teichmann (1999), Liston (1999), Panin and Tetzlaff (1999), and Van Breugel *et al.* (1999). Rodriguez-Camino and Avissar (1999) discuss the use of *effective parameters* to describe surface heat fluxes in heterogenous terrain. They conclude that nonlinear relations provide more accurate representations of the surface fluxes than does linear averaging.

The concept of an effective parameter assumes that an interpolation variable can be used to accurately represent area-averaged fluxes over a heterogenous landscape. This interpolation variable itself has no explicit physical realism (i.e., it cannot be directly measured or even diagnosed from point measurements). As shown by Rodriguez-Camino and Avissar (1999) and Ronda and De Bruin (1999), the relationship between most land-surface characteristics and surface heat fluxes are nonlinear. This makes the computation of effective parameters more difficult. Other papers that discuss the effective parameter approach include Hu *et al.* (1999).

Analytic and numerical modeling studies indicate that surface fluxes over heterogeneous flat terrain can be linearly weighted to compute area-averaged surface fluxes as long as the spatial scale of the landscape variations are smaller than about 5–10 km on a side (Dalu *et al.* 1991; Avissar and Schmidt 1998). This linear averaging of the surface fluxes is called the *mosaic approach*. These surface fluxes can be calculated using the theoretical basis for subgrid-scale parameterizations, as introduced in this chapter. On these spatial scales, it is assumed (as based on the model) that the surface fluxes *blend* into a homogeneous boundary layer above the surface layer. The heights at which this occurs is called the *blending height* (see, e.g., Goode and Belcher 1999). When the blending height is within or at the top of the surface layer, this necessarily means that the internal boundary layer is contained within the surface layer.

However, when the internal boundary layer is above the surface layer, the mosaic approach is necessarily inadequate. Variations in the boundary-layer depth can create mesoscale wind circulations (Dalu and Pielke 1993; Zeng and Pielke 1995a, b). Moreover, when internal boundary layers above the surface layer are important, parameterizations for subgrid-scale fluxes as used in all mesoscale and larger-scale models will have errors. *There is no parameterization of subgrid-scale fluxes that include the effects of such internal boundary layers.*

The presence of terrain elevation variability introduces an additional type of landscape variability (Gopalakrishnan and Avissar 2000). This elevation varia-

tion will accelerate and decelerate the wind flow, even in the absence of surface frictional effects, as represented by z_0. The effect of terrain variability on the flow is referred to as *form drag*. This topic was introduced in Section 5.3 and is discussed further in Section 12.5.3. With respect to large-scale models, form drag is discussed in Palmer *et al.* (1986), and McFarlane (1987).

The results of Panofsky *et al.* (1981, 1982) suggest that the turbulence spectra of airflow over complex terrain rapidly reaches an equilibrium with the new topography for wavelengths that are short compared to the fetch over the new terrain. Since the vertical velocity spectra generally contain less long-wavelength energy than the horizontal velocity spectra, it tends to reach equilibrium faster. Over hilly terrain, the long-wavelength portion of the horizontal velocity spectra, which is normal to the topography, loses energy to the horizontal terrain-parallel flow and to vertical motion. This change in the energy within the individual components results from the distortion of the mean flow by the terrain. Højstrup (1981) reached the conclusion that the adjustment of the low frequencies to changing terrain may require hours, so that in reality an equilibrium for these long wavelengths is never achieved.

Other studies of the influence of terrain on boundary-layer airflow include the wind tunnel studies by Britter *et al.* (1981), Pearse *et al.* (1981), and Neal *et al.* (1982); the numerical modeling simulations of a two-dimensional ridge by Taylor (1981) and of a three-dimensional isolated hill in Alberta by Walmsley *et al.* (1982); the analytic study of Jackson and Hunt (1975); and the observational studies of Camuffo (1982). Hunt and Simpson (1982) summarize the understanding of the change in boundary-layer structure as air advects over irregular terrain and other differential surface characteristics. Roth (2000) discusses how the boundary layer within about three times the height of buildings in cities is not adequately represented by standard boundary-layer parameterizations (such as discussed in this chapter and used by all existing mesoscale models). Clearly, this is an aspect of the models that needs improvement.

In any case, the current lack of alternative parameterizations for the boundary layer in heterogeneous nonsteady conditions requires that *only theory developed for horizontally homogeneous steady-state boundary layers are available for use in mesoscale models to represent subgrid-scale fluxes.*

Notes to Chapter 7

1. In this example, and in actual measurements, upward motion does not always transport warmer air aloft even if the ground is warmer, because cooler air mixed downward at an earlier time or different location may be entrained in an upward-moving region.

2. This is essentially the Boussinesq approximation. See Chapter 4 following Eq. (4-15) for a description of this assumption.

3. The Reynolds assumption; see following Eq. (4-8).

4. Although the reference to Eq. (7-5) as a turbulent kinetic energy equation is relatively standard, it is imprecise to do so, since molecular viscosity [e.g., Eq. (3-29)] was ignored in the original equations [e.g., Eq. (2-45)]. Therefore, molecular dissipation of turbulent energy is excluded in Eq. (7-5).

5. It is important to note that the averaging operation given by Eq. (4-6) is not the same as that used in turbulence theory. Standard turbulence observations involve measurements at specific points on a tower or along an aircraft track. In the first case, averaging is in time, whereas in the second case a one-dimensional space average is used. The parameterization of subgrid-scale fluxes, however, uses the results from these observational studies, as discussed in this chapter. Such an equivalence is justified only if the measured turbulence characteristics are essentially the same as those occurring throughout the averaging grid volume. Porch (1982) presented an example of a comparison of volume averaging (using an optical anemometer) and a point measurement (a cup anemometer) for a drainage flow observational study in a California valley. He concluded for that study that point measurements should be averaged for a relatively long time (around 2 hours) to represent more accurately the volume-averaged values. Unfortunately, of course, if the spatial variations are too large across the volume, then no amount of time averaging at a point can provide the appropriate average.

6. A discussion of the number of grid points required to resolve such a range of scales is given at the beginning of Chapter 4.

7. Schmidt and Housen (1995) provide a useful summary of the use of dimensional analysis in geophysical problems.

8. Weber (1999) discusses alternative definitions of the friction velocity.

9. $[\overline{w''u''}\frac{\partial \bar{u}}{\partial z}+\overline{w''v''}\frac{\partial \bar{v}}{\partial z}]=-u_*^2[\cos\mu\frac{\partial \bar{u}}{\partial z}+\sin\mu\frac{\partial \bar{v}}{\partial z}]=-u_*^2[\cos^2\mu\frac{\partial \overline{V}}{\partial z}+\sin^2\mu\frac{\partial \overline{V}}{\partial z}]=-u_*^2\frac{\partial \overline{V}}{\partial z}$.

10. Hicks and Everett (1979) commented that the displacement height could be different for each of the dependent variables in Eq. (7-34). However, since additional research is needed to ascertain whether this is true, in this section D is treated the same for all variables.

11. A somewhat different formation given by $\overline{V}=\overline{V}_D\exp a[(z/D)-1]$ is often used. However, with this expression, $\overline{V}_D$ does not equal 0 at $z=0$, as it should. Pinker and Moses (1982) have given an example of the estimation of the flow within an evergreen tropical forest using this formulation.

12. Traditionally, this layer was called a "laminar sublayer," although, as evident in Eq. (7-39), turbulent fluxes still occur within $z<z_0$ since u_*, q_*, and χ_* still appear.

13. When a zero-plane displacement D is required, the formulation given by Eq. (7-34) must be used. Also, in this section, only the flux of water vapor (i.e., $n=3$) is discussed.

14. The deposition velocity, as reported by, for example, Galloway *et al.* (1980), is dependent on the rate of uptake of the gas or aerosol by vegetation, the speed of transfer through the laminar layer just above the leaf surfaces of the vegetation, and the intensity of turbulent mixing at the top of the vegetation.

15. This was estimated by R. Pearson, Jr., CSU (1982, personal communication).

16. In the context of a model, the height of the planetary boundary layer is the grid-area (i.e., $\Delta\tilde{x}^1$ by $\Delta\tilde{x}^2$)–averaged depth z_i, to which the grid-volume–averaged fluxes of heat, momentum, moisture, and pollutants extend *through the transfer of mass*.

17. Roll vortices also can occur in neutrally stratified boundary layers. In a neutral boundary layer, roll vortices obtain their kinetic energy from vertical shear of the horizontal wind, whereas in inversion-capped heated boundary layers, the energy is derived primarily from buoyancy (see, e.g., Mason and Sykes 1980, 1982).

18. $\overline{w''_{z_i}\theta''_{z_i}}/\Delta\bar{\theta}_i=\overline{w''_{z_i}(\theta''_{z_i}/\Delta\bar{\theta}_i)}=\overline{w''_{z_i}(\rho''_{z_i}/\Delta\bar{\rho}_i)}$ as long as $|\theta''_{z_i}|\ll\Delta\bar{\theta}_i\ll\bar{\theta}_0$.

19. Some investigators (e.g., Mailhot and Benoit 1982) define first-order closure as meaning that an exchange coefficient is used to represent the subgrid-scale fluxes [see, e.g., Eq. (7-7)]. In this text, however, first-order closure means that the exchange coefficients must be defined *only* in terms

of the grid-volume–averaged dependent variables and *not* by averages of the higher moments of the subgrid-scale fluctuations, such as the grid-volume–averaged subgrid-scale kinetic energy $\frac{1}{2}\overline{u_i''^2}$.

20. The 0.01 uncertainty in the value of k [see the text before Eq. (7-19)], results in an uncertainty in C_D and, therefore, the fluxes that can be as large as 10% ($\overline{u''w''} = -u_*^2 \sim -k^2$).

21. In the surface layer, when Ri = 0, Eq. (7-57) should reduce to $K_m = ku_*z$ [Eq. (7-18)]. Substituting Eq. (7-19) for $|\partial V/\partial z| = \partial \overline{V}/\partial z$ in Eq. (7-57), yields $K_m = 1.1\,ku_*z$ however. Thus the reason for the coefficient 1.1 in Eq. (7-57) is not clear. In addition, from Eq. (7-33), K_m and K_θ are not equal at Ri = 0 in the surface layer. Finally, as discussed by Gutman *et al.* (1973), the vertical derivative of the horizontal wind vector, rather than the vertical derivative of the wind speed, should be used in Eq. (7-57) unless the wind direction is invariant with height.

22. A minimum of two grid lengths are needed to represent even a portion of a feature in a model, and at least four grid lengths are required for somewhat accurate resolution in the conservation equations, as discussed in Chapter 10.

Additional Readings

To understand the parameterization techniques for representing the subgrid-scale fluxes used in mesoscale models, it is necessary to understand atmospheric turbulence. Among the valuable texts in this area are the following:

Lumley, J. L., and H. A. Panofsky. 1964. "The Structure of Atmospheric Turbulence." Interscience Monographs and Texts in Physics and Astronomy, Vol. 12, Interscience, New York.
John Lumley wrote the first half of this classic book, and Hans Panofsky wrote the second. Lumley's sections provide the mathematical basis for turbulence theory, and Panofsky's portion emphasizes specific applications of this theory to an improved understanding of mixing in the atmosphere.

Tennekes, H., and J. L. Lumley. 1972. "A First Course in Turbulence." MIT Press, Cambridge, MA.
The authors introduce turbulence theory using effective physical examples of such mixing. This text is a valuable reference source for nomenclature and clear explanations of turbulence theory.

The following contributions provide excellent in-depth discussions on how to parameterize the atmospheric boundary layer.

Bélair, S., J. Mailhot, J. W. Strapp, and J. I. MacPherson. 1999. An examination of local versus nonlocal aspects of a TKE-based boundary layer scheme in clear convective conditions. *J. Appl. Meteor.* **38**, 1499–1518.

Beljaars, A. C. M., and P. Viterbo. 1998. Role of the boundary layer in a numerical weather prediction model. In "Clear and Cloudy Boundary Layers," A. M. Holstlag and P. G. Duynkerke, Eds., Royal Netherlands Academy of Arts and Sciences, Amsterdam., 287–304.

Blackadar, A. K. 1979. High-resolution models of the planetary boundary layer. "Adv. Environ. Sci. Eng.," **I**, J. R. Pfafflin and E. N. Ziegler, Eds., Gordon and Breach Science Publishers, 50–85.

Cuijpers, J. W. M., and A. A. M. Holtslag. 1998. Impact of skewness and nonlocal effects on scalar and buoyancy fluxes in convective boundary layers. *J. Atmos. Sci.* **55**, 151–162.

Eugster, W., W. R. Rouse, R. A. Pielke Sr., J. P. McFadden, D. D. Baldocchi, T. G. F. Kittel, F. S. Chapin III, G. E. Liston, P. L. Vidale, E. Vaganov, and S. Chambers. 2000. Land-atmosphere energy exchange in Arctic tundra and boreal forest: Available data and feedbacks to climate. *Global Change Biology*, **6**, 84-115.

Garratt, J. R. and G. D. Hess. 2001. The idealized neutrally stratified planetary boundary layer. In "Encyclopedia of Atmospheric Sciences," J. Holton and P. Taylor, Eds., Academic Press, London.

Holtslag, A. A. M. 1998. Fluxes and gradients in atmospheric boundary layers. In "Clear and Cloudy Boundary Layers," A. A. M. Holtslag and P. G. Duynkerke, Eds., Royal Netherlands Academy of Arts and Sciences, Amsterdam.

Moran, M. D. 2001. Basic aspects of mesoscale atmospheric dispersion. In "Mesoscale Atmospheric Dispersion," edited by Z. Boybeyi, Vol. 9, Advances in Air Pollution Series. Wit Press, Ashurst, Southampton, United Kingdom.

Uliasz, M. 1994. Subgrid scale parameterizations. In "Mesoscale Modeling of the Atmosphere," R. Pearce and R. A. Pielke, Eds., 13–19, American Meteorological Society, Boston, MA.

Velho, H. F. C., R. R. Rosa, F. M. Ramos, R. A. Pielke Sr., G. A. Degrazia, C. Rodrigues Neto, and A. Zanandrea. 2001. Multifractal model for eddy diffusivity and counter-gradient term in atmospheric turbulence. *Physica A*, **295**, 219–223.

Vermeulen, J. P. L. 2001. The atmospheric boundary layer over a heterogeneous vegetated landscape. Ph.D. Thesis, Vrije University, Amsterdam, 164 pp.

There are a series of excellent books on boundary-layer theory. The following texts are among the best.

Arya, S. P. 1988. "Introduction to Micrometeorology." Academic Press, San Diego.

Garratt, J. R. 1992. "The Atmospheric Boundary Layer." Cambridge University Press, Cambridge, U.K.

Garstang, M., and D. Fitzjarrald. 1999. "Observations of Surface to Atmospheric Interactions in the Tropics." Oxford University Press, New York.

Holtslag, A. A. M., and P. G. Duynkerke. 1998. "Clear and Cloudy Boundary Layers." Royal Netherlands Academy of Arts and Sciences, Amsterdam.

Sorbjan, Z. 1989. "Structure of the Atmospheric Boundary Layer." Prentice-Hall, Englewood Cliffs, NJ.

Stull, R. B. 1988. "An Introduction to Boundary Layer Meteorology." Kluwer Academic Publishers, The Netherlands.

Stull, R. B. 2000. "Meteorology for Scientists and Engineers." 2nd ed., Brooks/Cole Thomson Learning.

A very useful summary of field campaigns and long-term observational facilities to monitor the boundary layer is reviewed in Tunick (1999). Recent valuable review papers include Avissar (1995) and Brutsaert (1998).

Problems

1. Select a parameterization for the subgrid-scale heat fluxes from an atmospheric model of your choice. Dissect the parameterization using the technique outlined in Section 7.3.3.3. List the additional new dependent variables, and adjustable and universal parameters. Assess the sensitivity in the calculated value of the flux for uncertainties of $\pm 10\%$ as a function of one or more of the adjustable constants and universal parameters.

2. Perform problem 1, except for the subgrid-scale parameterization used for the velocity fluxes. What are the differences between the two parameterizations?

3. Derive an equation in which $\overline{S_\phi''} = 0$ is not assumed.